View Article Online
View Journal

Journal of Materials Chemistry A

Materials for energy and sustainability

This article can be cited before page numbers have been issued, to do this please use: W. Liu, H. Li, E. Bekyarova, R. Y. Tay and A. Yu, *J. Mater. Chem. A*, 2026, DOI: 10.1039/D6TA00650G.

Volume 6
Number 12
28 March 2018
Pages 4883-5230

Journal of Materials Chemistry A

Materials for energy and sustainability

rsc.li/materials-a

ISSN 2050-7488

ROYAL SOCIETY OF CHEMISTRY

COMMUNICATION
Zhenhai Wen *et al.*
An electrochemically neutralized energy-assisted low-cost acid-alkaline electrolyzer for energy-saving electrolysis hydrogen generation

ROYAL SOCIETY OF CHEMISTRY

View Article Online
DOI: 10.1039/D6TA00650G

Stimuli-Responsive Materials-Based Smart Supercapacitors: Design, Progress, and Perspectives

Wenwen Liu,[a*] Hongling Li,[a] Elena Bekyarova,[b] Roland Yingjie Tay,[a*] Aiping Yu [c*]

[a] School of Electrical and Electronic Engineering, Nanyang Technological University, 50 Nanyang Avenue, Singapore 639798, Singapore

[b] University of California-Riverside, 900 University Ave, Riverside, CA 92521, United States

[c] Department of Chemical Engineering, Waterloo Institute for Nanotechnology, University of Waterloo, Waterloo N2L 3G1, Canada

*Corresponding Authors. E-mail address: wenwen.liu@ntu.edu.sg; rolandtay@ntu.edu.sg; aipingyu@uwaterloo.ca

Abstract

With the rapid development of portable/wearable electronics, it is highly desirable to develop the external stimuli-responsive (e.g., temperature, magnetic field, light, voltage) energy storage systems to meet the requirements of these devices. Among them, stimulus-responsive materials-based smart supercapacitors (SCs) have attracted much attention due to their combination of SCs advantages and specific responses to environmental stimuli. As a key component of such smart devices, stimuli-responsive materials play a significant role in the design of smart SCs. Despite some progress, the design, fabrication, and application of multi-responsive materials for building smart SCs are still in the early stages, especially regarding the effects of each force/stimulation on capacitor behavior. Therefore, it is vital to summarize the research works and developments, which are not only instructive for researchers in this field but also crucial for the development of other smart energy storage devices. In this scenario, our review timely summarizes the latest reported stimuli-responsive materials-based SCs, covering their fundamental principles, design strategies, and configuration as well as their capacitor behaviour correlated to external forces/stimulations. Particularly, the different ways in which external forces/stimulation can interact with the components of SCs are discussed. Furthermore, future perspectives and challenges in this field for the development of multi-responsive electrode-material-based smart SCs are highlighted. Additionally, it is expected that this summary will place stimulus-responsive SCs in practical applications and provide insights for the design of other smart energy storage devices.

Keywords: External stimuli force; Responsive materials; Smart supercapacitors; Capacitor behavior

1. Introduction

View Article Online
DOI: 10.1039/D6TA00650G

Currently, with the rapid development of novel wearable electronics and sensors, energy storage devices are required to possess characteristics such as lightweight design, mechanical flexibility, miniaturization, and environmental adaptability. However, traditional energy storage devices cannot fully satisfy these requirements.[1, 2] Therefore, it is necessary to explore appropriate energy storage systems to meet these new demands. Among them, stimuli-responsive materials-based smart supercapacitors (SCs) have received increasing attention.[3, 4] They not only inherit the advantages of SCs (e.g., excellent power density, long cycle life.) but also exhibit multi-functionality towards environment stimuli.[5, 6] As reported, the overall performance of SCs mainly depends on the electrode materials and/or electrolytes, so stimuli-responsive materials with the characteristics of interaction and/or self-regulation towards external stimuli play a significant role in the construction of smart SCs.[7-9] Therefore, researchers have made efforts to explore suitable stimuli-responsive materials and to design stimuli-responsive smart SCs.[10-14] Although the research in this related field is still in the early stages, progress has been made in recent years, and the research on this area has become a hot topic.[8, 15] More importantly, it is predicted that there will be a flourishing growth of the stimuli-responsive materials-based smart SCs in the next few years. Hence, it is necessary to summarize these research findings, progress, and breakthroughs, thereby providing useful guidance for this emerging field. However, systematic summaries of the specific applications of stimuli-responsive materials in smart SCs remain limited, despite their importance for guiding research in this field. Therefore, a comprehensive review is highly desired to summarize the recent progresses in the design and construction of stimuli responsive smart SCs, with particular emphasis on the specific effects of external force/stimulation on the electrochemical performance.

Bearing this in mind, our review paper timely fills the gap and primarily covers the design of external stimuli-responsive materials/electrolytes, as well as the appropriate application of these forces/stimuli to design stimuli-responsive SCs. First, the background and motivation for the development of external-stimuli-responsive smart SCs are briefly introduced. Then, the principles of stimuli-response materials and their responsive properties are presented. Next, the latest progress in stimuli-responsive materials-based smart SCs in responding to various external stimuli (e.g., temperature, magnetic field, light, voltage) is systematically summarized. This paper delves into the specific effects of external force/stimulation on the electrochemical performance of SCs, particularly the different ways in which external forces/stimuli interact

View Article Online
DOI: 10.1039/D6TA00650G

with the various components. Furthermore, future perspectives and challenges in the construction of stimuli-responsive materials-based smart SCs are discussed. This review not only provides insights into the development of such smart SCs but also offers useful guidance for the design of other smart energy storage devices and inspires innovative concepts for future research.

2. Design of stimuli-responsive electrode/electrolyte materials

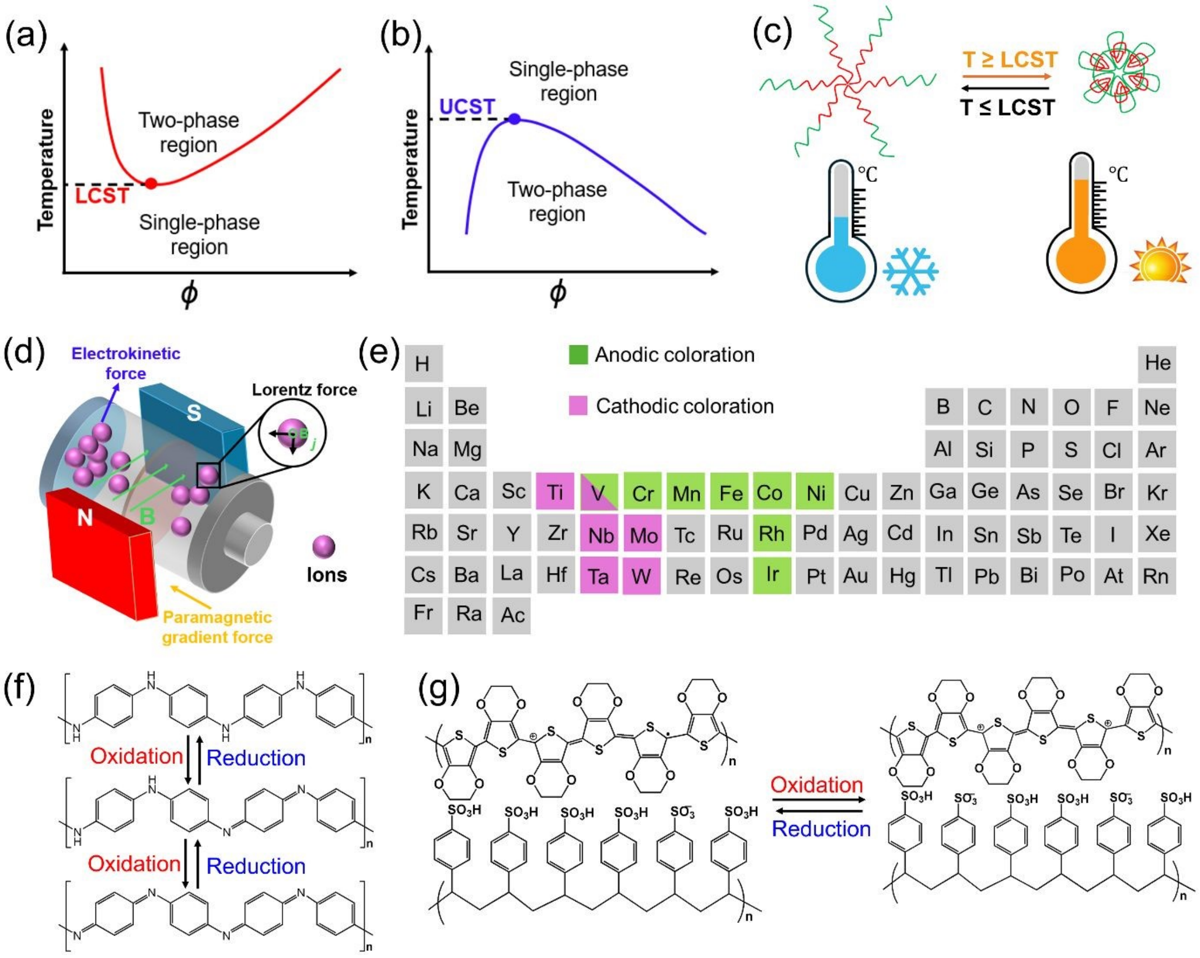

Figure 1. Phase diagram for polymer/solvent mixtures with different thermos-responsive behaviors: (a) LCST, (b) UCST, respectively. (c) Illustration of the structure change of the polymer electrolyte with LCST during the heating/cooling cycle. (d) Illustration of main body forces generated on SCs in a magnetic field. (e) Anodic coloration and cathodic coloration related to transition metal oxides. Electrochromic mechanism of (f) PANI and (g) PSS-PEDOT, respectively.

Table 1. Comparison of advantages and disadvantages of different external forces/stimulations-based smart SCs.

Stimulus type	**Mechanism**	**Key advantages**	**Key disadvantages/challenges**
Temperature	Material functional properties (e.g., hydrophilic-hydrophobic property, electrical conductivity) change significantly when the temperature exceeds a certain threshold.	Reversibly switching off capacitance when overheating and automatically restoring function upon cooling; absorbing/releasing heat during phase transitions and stabilizing internal temperature and performance in both low and high conditions; improving energy density through voltage extension; exhibiting good mechanical stability under deformation.	Complex material engineering to create stable dual-zone phase-change materials; slower physical phase transitions causing slow response time; non-conductive phase change materials or thermally-gating polymers reducing the electrode’s conductivity or overall specific capacitance.
Magnetic field	The co-existence of electric current and changes in electric field were usually accompanied by the generation of a magnetic field.	Manipulating ions without physical connections; accelerating ion transport at the electrode interface for fast charging/discharging; aligning electrodes for better performance during fabrication.	Early research stage with limited real applications; incorporating magnetic materials, resulting in complexity and high cost; unclear fundamental mechanisms.
Light	When light hits a photoactive electrode, it excites electrons, creating electron-hole pairs. These charges are then separated, in which electrons are stored at the electrode interface and holes participates in reactions, thus boosting charge storage capability.	Reducing external charging and creating self-powered device; enabling novel features to be integrated into displays and other devices.	Integrating light-harvesting and storage modules, thus leading to lower photovoltaic conversion efficiency and internal resistance; complex design process for effective photoactive electrodes with suitable band gaps, efficient charge separation, and long-term stability; easily recombing photogenerated charge carriers before being stored.

Voltage	It is a fascinating synergy where energy storage and color changes happen simultaneously, where they leverage a single electrochemical reaction to perform both capacitor function and electrochromic function.	Ability to visually indicate energy storage levels in real time; Combining energy storage modulation and optical modulation, which is ideal for smart windows and displays.	Material compromise because electrode materials must excel at both energy storage and electrochromic; slow response time limiting practical application; repeated color switching and charge/discharge cycles causing materials degradation, delamination and performance fading; difficulty in balancing optical contrast, coloring efficiency, energy density, and cycle life.

Stimuli-responsive materials, that change their properties or states in response to external stimuli (e.g., temperature, magnetic field, light, voltage), are also denoted as "smart materials",[16, 17] which are highly desirable in various applications, such as memory devices, artificial muscles, and energy storage systems (**Figure 1**).[18, 19] This inherent responsiveness allows for the development of adaptive and controllable electrochemical devices like sensors, actuators, and SCs.[20-25] Among them, the stimuli-responsive behavior of SCs stems from the fundamental interaction between the designed electrode/electrolyte and external forces/stimuli (**Table 1**). Stimuli-responsive material is a key component of smart responsive SCs, which has spurred the development of various strategies to design and synthesize different materials/components with unique responsive properties.[26-30] To better understand the internal logic of the design of smart SCs based on these stimuli-responsive materials, we briefly introduce the working principle of these materials interacting with the external stimuli such as temperature, magnetic field, light, and voltage, and outline the effects of these external stimuli on their capacitor behavior.

2.1 Temperature-responsive materials-based SCs

Most thermoresponsive materials are smart polymers whose functional properties (e.g., hydrophilic-hydrophobic property, electrical conductivity) change significantly when the temperature exceeds a certain threshold, known as the critical solution temperature.[31-33] These changes effectively suppress ion or electron conduction between electrodes. Generally, the thermo-responsive behavior can be classified into two types: lower critical solution temperature (LCST) (**Figure 1a**) and upper critical solution temperature (UCST) (**Figure 1b**),[34-36] respectively. The LCST referred to the temperature above which the polymer separated and became turbid due to its reduced solubility, while the solution became clear and transparent again below the LCST. Regarding the UCST, it referred to the temperature at which the polymer became insoluble, and phase separation occurred. Here, LCST thermo-responsive polymers (e.g., poly(N-isopropylacrylamide) (PNIPAM) and its derivatives) were used as examples to illustrate their working principles (**Figure 1c**). Below the LCST, the polymers absorbed water, swelled, and became hydrophilic. Conversely, above the LCST, hydrophobic interactions dominated, forcing water to escape, causing the polymer to collapse and becoming hydrophobic. The reversible temperature-triggered behavior led to significant changes in ion transport and/or conductivity, making them ideal materials for designing thermos-responsive SCs.

Recently, thermal-responsive polymers (e.g., PNIPAM[37-39] and its copolymer (NIPAM copolymerized with acrylic acid (AA)[11, 40], acrylamide (AM)[26, 41] and methylcellulose (MC)[42, 43]) were employed to design the thermal-responsive smart SCs and other energy storage devices. As reported, the thermo-responsive smart SCs can be achieved by integrating thermo-responsive polymers in SCs components (e.g., electrode materials, electrolytes) based on different functional mechanisms.[44] From a material perspective, a common strategy for designing thermoresponsive smart SCs was to integrate the thermoresponsive materials into electrodes.[45] These thermoresponsive electrodes consisted of conductive fillers and a specific polymer with a large coefficient of thermal expansion. When increasing the temperature, the volume expansion of the polymer increased the distance between conductive fillers, which resulted in a few orders of magnitude decrease in the conductivity of the thermoresponsive electrode. There was no doubt that the fast and reversible thermoresponsive electrodes with self-adjustable conductivity enabled the conductive filler/polymer composites to be promising materials for the design of thermoresponsive smart SCs. Moreover, the modification of electrode materials with thermo-responsive polymers was also employed to construct the smart thermo-responsive SCs.[27] In this scenario, the thermoresponsive polymer acted as a valve to promote and prevented the diffusion of electrolyte ions through its configuration changes under cooling/heating conditions. This general and promising approach can be extended to functionalize other components of SCs, thus enabling the obtained smart SCs with thermal responsibility. Apart from the design of the thermoresponsive electrodes, another strategy was to explore the thermoresponsive electrolyte to control ion diffusion under different temperature conditions.[11, 26] The thermally responsive electrolytes with reversible sol-gel transition phases have attracted widespread attention. The sol-gel transition process was determined by the LCST, which had a significant impact on the electrolyte ion diffusion rate. When the temperature was above the LCST, the polymer molecular chains formed micelles, which generated a gel network due to hydrophobic interactions, thus suppressing the free migration of ions. When the temperature was below LCST, the strong hydrogen bonding between the polymers and the solvent molecules led to polymer dissolution, thereby facilitating the migration of ions.[22, 44]

2.2 Magnetic-responsive materials-based SCs

Clearly, magnetic fields affected electrochemical processes, but the underlying mechanism of these effects was a cross-disciplinary concept involving physics, chemistry, material science, electrochemistry, and magnetism. In this case, a better understanding of the effect of the

View Article Online
DOI: 10.1039/D6TA00650G

external magnetic field on the electrochemical behavior of the SCs device could lead to significant breakthroughs in the design of high-performance magnetic-responsive SCs. From a physics point of view, according to Faraday's law of electromagnetic induction, the co-existence of electric current and changes in electric field were usually accompanied by the generation of a magnetic field.[46-49] Generally, the main driving forces for the movement of electrolyte ions during the charge/discharge processes were electromigration, diffusion, and convection. However, when a magnetic field was applied, there were five extra body forces introduced (**Figure 1d**),[48] which included the paramagnetic gradient force (F_p), field gradient force (F_B), Lorentz force (F_L), electrokinetic force (F_E) and magnetic damping force (F_M). The definition and calculation of these five body forces were briefly described as follows:

(a) Paramagnetic gradient force (F_p) was generated by the interaction between an applied magnetic field and the concentration gradient of paramagnetic species. It can be calculated by Equation (1):

$$\overrightarrow{F_p} = \frac{x_m B^2 \vec{\nabla} c}{2\mu_0} \qquad (1)$$

Where x_m, B, ∇, c, and μ_0 referred to the molar susceptibility, the magnetic field strength, the del operator, the concentration and the permeability of free space,[50, 51] respectively.

(b) Field gradient force (F_B) was a force that arose when a magnetic substance was placed in a non-uniform magnetic field. It was expressed as Equation (2):

$$\overrightarrow{F_B} = \frac{x_m c B \overrightarrow{\nabla \mathrm{B}}}{2\mu_0} \qquad (2)$$

Where x_m, B, ∇B, c, and μ_0 referred to the molar susceptibility, the magnetic field strength, the magnetic gradient, the concentration and the permeability of free space, [52, 53] respectively.

(c) Lorentz force (F_L) was the total electromagnetic force acting on a charged particle moving with velocity through electric and magnetic fields.[54] The Lorentz force was given by Equation (3):

$$F_L = q\,(E + v_d \times B) \qquad (3)$$

Where E, v_d, q and B was the electric field, the drift velocity, the charge, and the magnetic field strength, respectively.

View Article Online
DOI: 10.1039/D6TA00650G

(d) Electrokinetic force (F_E) referred to forces generated at the interface of a charged surface and a liquid, causing motion of particles or fluid due to electric fields.[54] The electrokinetic force (F_E) can be described by Equation (4):

$$\overrightarrow{F_E} = \sigma_d \overrightarrow{E_{\parallel}} \tag{4}$$

Where σ_d was the total charge density in the diffuse layer, and $E_{\parallel}$ was the effective electric field.

(e) Magnetic damping force (F_M) was a non-contact force that slowed or stopped the motion of a conductor by converting its kinetic energy into heat, generated by eddy currents induced when the conductor moved through a magnetic field. The magnetic damping force was given by Equation (5):

$$\overrightarrow{F_M} = \sigma \vec{v} \times \vec{B} \times \vec{B} \tag{5}$$

Where σ, v, and B were the conductivity of the conductor, the velocity of the magnet/conductor, and the magnetic field strength.[51, 54]

Based on the working principle of the SCs, their energy storage mechanism relied on the adsorption/desorption of electrolyte ions at the electrode/electrolyte interface or involved the surface redox reaction during the charge/discharge process. Nonetheless, compared with the fast electron transfer, the slow mass transport limited the performance (e.g., operating voltage, power density) of SCs. From this point of view, mass transport was considered one of the key processes,[55] typically controlled by diffusion and migration, while the contribution of convection was negligible.[56] In this case, an applied magnetic field provided an effective method to accelerate the mass transport. In short, when a magnetic field interacted with the ionic current in the electrolyte, convection was generated, thereby increasing the diffusional mass transfer rate and resulting in a narrower diffusion layer. The Lorentz force was reported to be the dominant magnetic force causing this effect.[55] Furthermore, when the field gradient force was comparable in magnitude to the Lorentz force, it was believed to have a similar effect on mass transport.[50-52, 57] In this case, when a magnetic field was applied to an electrochemical cell, convection effect through the ions' movement occurred due to the magnetohydrodynamic effect, thereby resulting in the decrease of the thickness of the diffusion layer and the enhancement of mass transport.[54] Additionally, the study found that the effect of the magnetic field on the performance of SCs was strongly dependent on the concentration and types of electrolytes used. [46]

View Article Online
DOI: 10.1039/D6TA00650G

According to the above discussion and analysis, a magnetic field can affect the electrochemical process in the following different ways: (1) modifying the properties of electrodes and/or electrolytes through the variation of the Hall effect and electrical conductivity; (2) controlling the mass transport *via* the superposition of the magnetic fields generated by the interaction of magnetohydrodynamic phenomena near the electrodes and the convective diffusion layer; (3) varying the electrochemical kinetics during the electrochemical process. In short, the magnetic field can influence the kinetics of electrolyte ions, electrode/electrolyte interactions, and the morphology and quality of the final product, thus providing a cherishing opportunity to design the magnetic field-responsive SCs.[54]

2.3 Light-responsive materials-based SCs

Light-responsive SCs are usually described as having a capacitive behavior that responds to light or can be tailored by harnessing light energy. Therefore, the light-driven SCs opened new possibilities for smart energy storage applications. The light-derived SCs included three-electrode photo-derived SCs and two-electrode photo-derived SCs,[58, 59] respectively. Generally, a three-electrode photo-derived SC has a dual-function intermediate electrode between the photoelectrode and the counter electrode, dividing the device into two sections: one for photoelectric conversion and the other for energy storage. For two-electrode photo-derived SCs, the design strategy was to integrate the energy generation and storage modules into a single device, thereby significantly simplifying the design and construction of photo-assisted charging SCs. Additionally, compared to three-electrode photo-derived SCs, the two-electrode system was a novel and compact system with advantages such as ease of assembly, low cost, and good cycling stability. Therefore, the photo-derived SCs presented in this review focused on the two-electrode photo-SCs unless otherwise mentioned.[60]

Light-responsive materials-based SCs utilize photo-generated holes/electrons on the surface of the photoelectrode to participate in energy storage. Concisely, when the photoactive materials are exposed to light, they generate electron-hole pairs. The rapid separation and transfer of these photogenerated charges enabled them to enhance the electric double-layer formation or participate in the reversible faradaic redox reactions. Therefore, light irradiation can boost the capacitance by increasing carrier density, promoting interfacial polarization, or driving charge transfer in engineered heterojunctions. In this system, light was applied to drive the photo-responsive materials by providing adjustable radiation energy. To interact with the light irradiation, the photo-responsive materials for light-assisted SCs should owned both the

View Article Online
DOI: 10.1039/D6TA00650G

photosensitive and pseudocapacitive properties. The ideal electrode materials should meet the following requirements: (1) an appropriate band gap to absorb more light; (2) a high separation efficiency of photo-generated electrons and holes. Among them, the semiconducting materials seemed to be the preferred options to design the photo-assisted smart SCs.

2.4 Potential responsive materials-based SCs

Currently, the design of smart SCs with electrochromic properties and good capacitive behavior have attracted tremendous interest. Generally, the electrochromic behavior resulted from the redox reactions between the electrode material and the inserted ions under applied voltage.[61,62] It was worth noting that pseudocapacitors also relied on the reversible redox reaction of materials. Therefore, combining electrochromism and energy storage capabilities to manufacture electrochromic energy storage devices was an excellent choice for designing voltage-responsive smart SCs. Electrochromic material, as an important component of electrochromic smart SCs, can be divided into three types: inorganic materials, organic materials, and hybrid materials. Owing to their different coloration mechanisms, these three types of electrochromic materials displayed different electrochromic properties in terms of response speed, color variation, and stability.

2.4.1 Mechanism of inorganic materials

Among these inorganic oxides, metal oxides were the most used electrochromic materials, such as WO_3, V_2O_5, MoO_3, Nb_2O_5, NiO, and MnO_2.[63, 64]. It is noted that different electrochromic materials exhibited quite diverse color-change potential range, by which the electrochromic materials can be split into two types: anodic and cathodic electrochromic materials (**Figure 1e**), respectively. Generally, the cathodic metal oxide materials were colored due to the insertion of electrolyte ions during the reduction process, while the anodic metal oxide materials were colored because of the extraction of corresponding ions during the oxidation process. The cathodic metal oxide materials, such as MoO_3, WO_3, possessed the unpaired single electron in the *d* orbital, which was beneficial for the cathodic charge injection, thus leading to the reversible change of valence state and inducing the reversible color change. Here, WO_3, a widely studied transition-metal oxide, was used as an example to reveal the color-change mechanism of cathodic electrochromic materials. The coloration and blenching processes of WO_3 were attributed to the insertion/extraction of cations, which can be explained as follows:

$$WO_3\ (Colorless) + xM^+ + xe^- \leftrightarrow M_xWO_3\ (Blue) \qquad (6)$$

View Article Online
DOI: 10.1039/D6TA00650G

Where M^+ referred to the cations (e.g., H^+, Li^+), and x value was between 0 and 1. Moreover, the electrochromic properties (e.g., coloration efficiency, switch speed, stability) of the WO_3 were also associated with the crystallinity.[20, 65]

On the other hand, anodic coloring effects can be seen in NiO, MnO_2, and Co_3O_4. These metal oxides were typically used as counter electrodes, combining with cathodic electrochromic electrodes to form devices. As a representative anodic coloration material, the reversible color change mechanism of NiO_x was shown as follows:

$$NiO_x + \alpha Li^+ + \alpha e^- \rightarrow Li_\alpha NiO_x \qquad （7）$$

$$Li_\alpha NiO_x\,(Bleached) \leftrightarrow \gamma Li^+ + \gamma e^- + Li_\beta NiO_x\,(Colored) \qquad （8）$$

Where $\alpha = \beta + \gamma$. Obviously, the color change of NiO_x was due to the intercalation/deintercalation of Li^+, which caused the change of valence state. Additionally, it was interesting to note that vanadium oxides can be used as both cathodic electrochromic materials and anodic electrochromic materials. Such a bifunctional electrochromic properties enabled their multicolor change properties.[66] Besides, apart from the above-mentioned metal oxides, metal complexes, such as Prussian blue, metal phthalocyanine, and their derivatives, were another type of inorganic electrochromic materials, which exhibited multicolor switching property. The color change of the metal complexes was related to the redox reaction of center metal ion as well as the involved ligands.[67-69]

2.4.2 Mechanism of organic materials

Except for inorganic materials, organic materials, such as organic molecules, conjugated polymers, and metal organic chelates, also showed electrochromic characteristics by offering multiple colors under different applied biases. Among these organic materials, small molecules such as viologens and anthraquinones were widely used as electrochromic materials due to their multi-color properties under different potentials.[70] Particularly, viologens (1,1′-disubstituted-4,4′-dipyridinium salts), a well-studied species with three reversible redox states, exhibited good electrochromic properties.[71] Furthermore, the nitrogen substituents (-R1 and -R2) in its molecule structure can be modified and thus enable the resulting viologens with diverse colors.[21]

In addition, conjugated polymers, which were another broad class of polymers with alternating single/double bonds, such as polyaniline (PANI), Poly(3,4-ethylenedioxythiophene)-poly(styrene sulfonic acid) (PEDOT:PSS), offered fast switching,

View Article Online
DOI: 10.1039/D6TA00650G

high efficiency, and varied colors. Depending on the applied potential and the doping states, the conjugated polymer can show different colors.[63] As a typical conjugated polymer, PANI exhibited the reversible multicolor change due to the anion injection/extraction process (**Figure 1f**).[72] PEDOT:PSS, as another typical cathodic electrochromic material, had also caused great interest, and its corresponding electrochromic mechanism was shown in **Figure 1g**. During the negative scan, the doping of electrolyte ions into the polymer backbone, causing the color to change from light blue to dark blue,[73, 74] while the color returned to the light blue because of the de-doping process on the reverse scan, thus achieving electrochromic properties.

3. Various stimuli-responsive SCs

SCs can be engineered to respond to external stimuli (e.g., temperature, magnetic fields, light, and voltage), thus achieving intelligent functionality.[75,76] For example, photostimuli-responsive SCs can reversibly change their capacitance by adjusting charge transfer at the interface under light, thus functioning as light-controlled switches for energy storage. These stimulus-responsive “smart” SCs can change their electrical or physical properties in real time, going beyond simple energy storage devices. Typically, the design of stimulus-responsive SCs involves the interdisciplinary integration of multiple disciplines. The related common processes for the construction of smart SCs can be summarized as follows: (1) determine the external stimulus required for the SCs based on the specific application; (2) select appropriate stimulus-response materials; (3) organically integrate the stimulus-response materials into the electrode structure design; (4) characterize and evaluate the performance of the stimulus-response electrodes/electrolytes and the fabricated SCs. This section mainly focuses on the representative examples for the design and preparation of various stimuli-responsive materials using different methods and precursors, and their application in constructing SCs that respond to specific external stimuli such as temperature, magnetic field, light, and voltage.

3.1 Temperature-responsive SCs

Stimuli-responsive polymers usually alter their properties (e.g., solubility, ion transport, conductivity) when the external temperature exceeds a certain threshold, known as the critical solution temperature. The reversible temperature-triggered behavior led to significant changes in their physicochemical properties, making them ideal materials for designing thermos-responsive SCs applications. From an application perspective, dual thermally responsive polymers exhibiting LCST or UCST behavior were attractive because they possessed the potential to be designed into smart materials that responded within a range of specific

View Article Online
DOI: 10.1039/D6TA00650G

environmental variables.[35] In this case, these polymers showed temperature LCST or UCST, which enabled them suitable for the design of thermoresponsive smart components, thus building the thermoresponsive smart SCs. Currently, these thermoresponsive polymers can be divided into three categories: (i) PNIPAM-based polymers, (ii) poly(ethylene oxide) (PEO)/poly(propylene oxide) (PPO)-based polymers, and (iii) cellulose derivatives,[34, 77] respectively.

3.1.1 PNIPAM-based polymers for temperature-responsive SCs

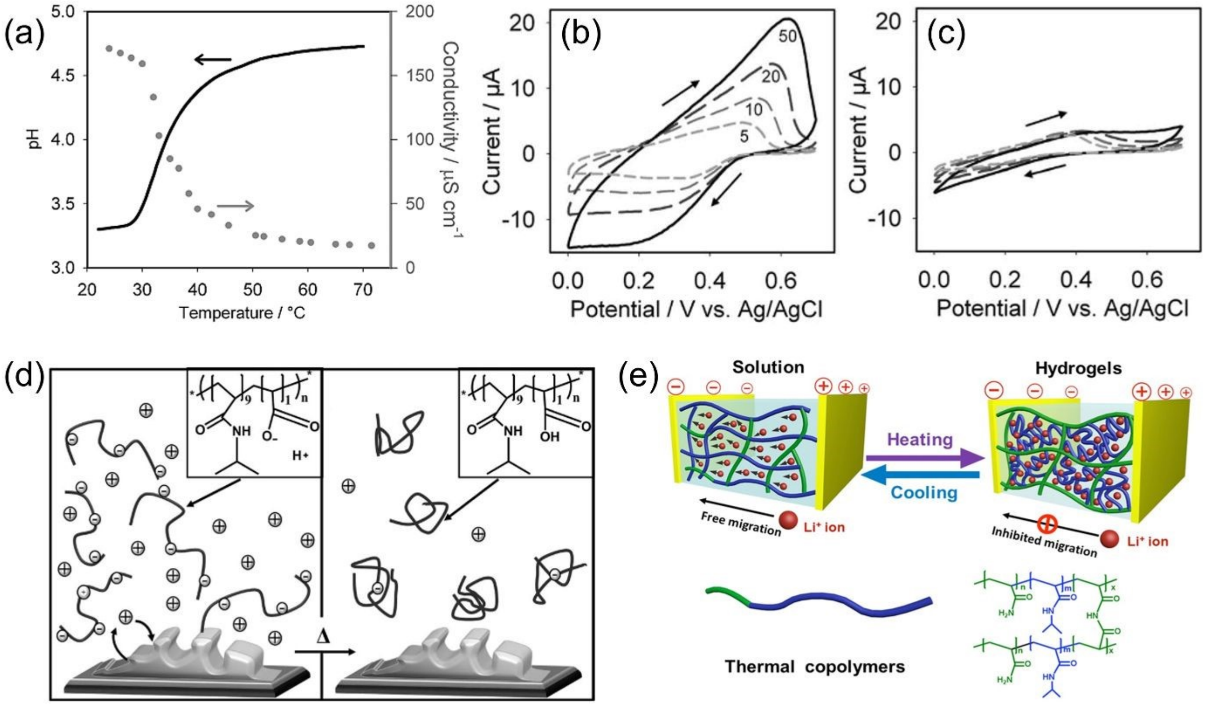

Figure 2. (a) Ionic conductivity of the optimized PNIPAM-AA copolymer electrolyte. CV curves of PANI in the optimized PNIPAM-AA copolymer electrolyte at (b) 22 °C and (c) 50 °C, respectively. (d) Illustration of the phase change of PNIPAM-AA copolymer at room temperature (Left) and temperature above the LCST (Right).[11] Reproduced with permission.[11] Copyright 2012, Wiley-VCH. (e) Illustration of sol–gel transition of LiOH–PNIPAM/AM electrolyte during the heating/cooling cycles.[26] Reproduced with permission.[26] Copyright 2015, Wiley-VCH.

By integrating thermally responsive polymers in SCs components (e.g., electrodes, electrolytes, separators), the self-adjustment smart SCs can be achieved based on different functional mechanisms. PNIPAM was a water-soluble polymer famous for its thermoresponsive nature. Briefly, it exhibited hydrophilic properties when the temperature was below LCST (32℃), while it became hydrophobic and insoluble when the temperature was above LCST.[36] The temperature-dependent properties made it a promising candidate in the development of smart SCs. However, the relatively low LCST limited the operation temperature range of SCs and practical applications. In this case, it was necessary to explore a new system for performance improvement. As a pioneering research work, a reversible thermally responsive polymer based on PNIPAM and AA copolymers was designed as an electrolyte,[11] where PNIPAM governed the thermal properties, while AA provided the electrolyte ions. The thermal switching properties of this electrolyte were investigated (**Figure 2a**). With the increase of the temperature from 22 to 70 ℃, the color of PNIPAM-AA copolymer solution changed from clear and transparent to milky white with precipitate as well as accompanying with the decrease of the conductivity from about 180 to 20 $\mu S\cdot cm^{-1}$. Its corresponding electrochemical behavior under cooling and heating condition were studied by cyclic voltammetry (CV) curves (**Figure 2b, 2c**). When the electrolyte temperature increased from 20 to 50 ℃, the redox peaks of PANI electrode disappeared and the area surrounded by CV curve greatly decreased, which was attributed to a thermal activated phase transition occurred in the PNIPAM-AA copolymer, resulting in the decreased availability of electrolyte ions and reduced ion conductivity (**Figure 2d**). On the contrary, when the operating temperature cooled down, the redox peaks on the CV curve appeared again. This was because the polymer re-dissolved into solution and more sufficient free ions were involved in the PANI redox reaction. The recovery property suggested the reversible thermally responsibility of the polymer electrolyte, thus making it be used in smart SCs.

Inspiring by this groundbreaking research on the PNIPAM-based electrolyte, a series of PNIPAM-based thermoresponsive copolymer electrolytes were synthesized to construct the thermoresponsive SCs. Particularly, the thermoresponsive electrolytes with a reversible sol-gel transition phase versus temperature had a significant impact on the electrolyte ion diffusion rate, thus leading to the different electrochemical performance as well as making them promising candidates to build the temperature responsive SCs. As a representative example, a copolymer, poly(N-isopropylacrylamide-co-acrylamide) mixed solution of LiOH (LiOH–PNIPAM/AM),[26] was designed. Noted that the Li^+ diffusion coefficient in LiOH–PNIPAM/AM electrolyte significantly decreased when the working temperature increased from 20 °C to 70 °C. The decrease in the Li^+ diffusion coefficient was due to the formation of a 3D network structure by the hydrophobic association during sol–gel transition, which inhibited the Li^+ ion migration. Furthermore, the reversibility of thermally responsive SCs was

View Article Online
DOI: 10.1039/D6TA00650G

investigated by measuring the capacitance during the electrolyte heating/cooling cycles. After multiple sol–gel–sol transition cycles, there was no significant decrease in the capacitance, indicating its practical application. Herein, the reversibility of temperature-dependent structural evolution upon the temperature (**Figure 2e**) functioned as a thermal-gated behavior and controlled the migration of electrolyte ions, thus realizing the construction of the smart thermoresponsive self-adjustment SCs. Similarly, another thermal sensitive copolymer, poly (N-isopropylacrylamide-co-glycidyl methacrylate) (referred to as P(NIPAM-co-GMA)), was used as electrolyte for the construction of smart SCs.[37] It was observed that this electrolyte was in solution state at room temperature due to its hydrophilic characteristic, allowing the free movement of ions. However, at high temperatures the contraction of the copolymer chains caused the electrolyte to transform into a hydrophobic state, thus preventing ion migration. This process demonstrated an effective strategy replying on temperature to design the smart SCs.

Notably, most reported sol-gel transition electrolytes were liquid at room temperature, which presented numerous problems (e.g., encapsulation difficulties, liquid leakage), severely limiting their performance in practical applications.[41, 78] Hydrogel electrolytes were considered an effective solution to solve these problems. Furthermore, hydrogel electrolytes were also ideal for portable flexible energy storage devices. In view of this, a reversible thermos-responsive PNIPAM-co-N-methylolacrylamide (NMAM) hydrogel electrolyte was successfully synthesized by free-radical polymerization.[22] Noted that the discharge time of the obtained SCs based on NMAM hydrogel electrolyte gradually decreased with the gradual increase of the operating temperature from room temperature (148 s) to 70 °C (21 s), which indicated that the specific capacitance of the device dropped rapidly. Its specific capacitance kept the constant value during the heating/cooling cycle, highlighting a high reversibility of the polymer electrolyte. The temperature-dependent performance presented here was attributed to the off–on ion-transport channels of electrolyte during the heating/cooling cycle. At room temperature, the hydrogel electrolyte surface exhibited a uniform distribution of micropores formed by interconnected molecular chains (**Figure 3a**), which were approximately elliptical in shape, thus facilitating the ion transport. However, most of the micropores disappeared at 70 °C (**Figure 3b**), which was due to the closure of ion channels caused by molecular chain association. When the temperature returned to room temperature, the closed micropores reopened (**Figure 3c**), at which point the ion transport channels were unobstructed. With the similar idea, the ionic liquid cross-linked PNIPAM hydrogel electrolyte was synthesized by a

View Article Online
DOI: 10.1039/D6TA00650G

one-step in-situ polymerization (**Figure 3d**).[79] Noted that the capacitance of the device was around 102 F·g^{-1} at 25 °C while reducing to almost 0 at 60 °C (**Figure 3e**), while the corresponding capacitance recovered when the temperature cooled down to room temperature. The reversible thermoresponsive electrochemical behaviors can be explained as follows. When the operating temperature was higher than the LCST value, the PNIPAM polymeric chains formed a physical cross-linker, thus disrupting the original ion-conductive channels (**Figure 3f**). Meanwhile, the ionic liquid component also played an important role in confining the conductive ion in the polymer phase, thus accelerating the LCST effect on ion modulations and effectively controlling ion migrations. Undoubtedly, these two factors resulted in the significant decrease of the ion conductivities at 60 °C. This was supported by the diffusion coefficient of lithium ions decreasing from 5.97×10^{-11} m^2·s^{-1} at 25 °C to 2.72×10^{-13} m^2·s^{-1} at 60 °C.

Apart from the design of the thermoresponsive electrolytes, another feasible solution for the construction of thermoresponsive SCs was to directly integrate the thermoresponsive materials into electrodes from the material point of view. In view of this, a simple strategy was to load the thermosensitive polymer (e.g., P(NIPAM-co-SPMA)) onto the surface of NiAl-layered double hydroxide (referred to as LDH@P(NIPAM-co-SPMA) electrode) (**Figure 3g, 3h**).[27] Based on the discharge curves, its specific capacitance dramatically decreased from 518 F·g^{-1} at 20 ℃ to 38 F·g^{-1} at 40 ℃ (**Figure 3i**). The largely suppressed electrochemical capacitance at 40 ℃ was attributed to the closure of the ion transport channels. Also, noted that the specific capacitance quickly switched between 20 ℃ and 40 ℃ (**Figure 3j**), indicating a highly reversible transition of this composite electrode induced by the P(NIPAM-co-SPMA) polymer. This thermoresponsive polymer acted as a valve by changing its configuration under cooling/heating conditions, thus promoting and preventing the diffusion of electrolyte ions. Encouragingly, this general and promising approach can be extended to design other thermoresponsive electrodes and functionalize other components, thus enabling the obtained smart devices with thermal responsibility.

View Article Online
DOI: 10.1039/D5TA00650G

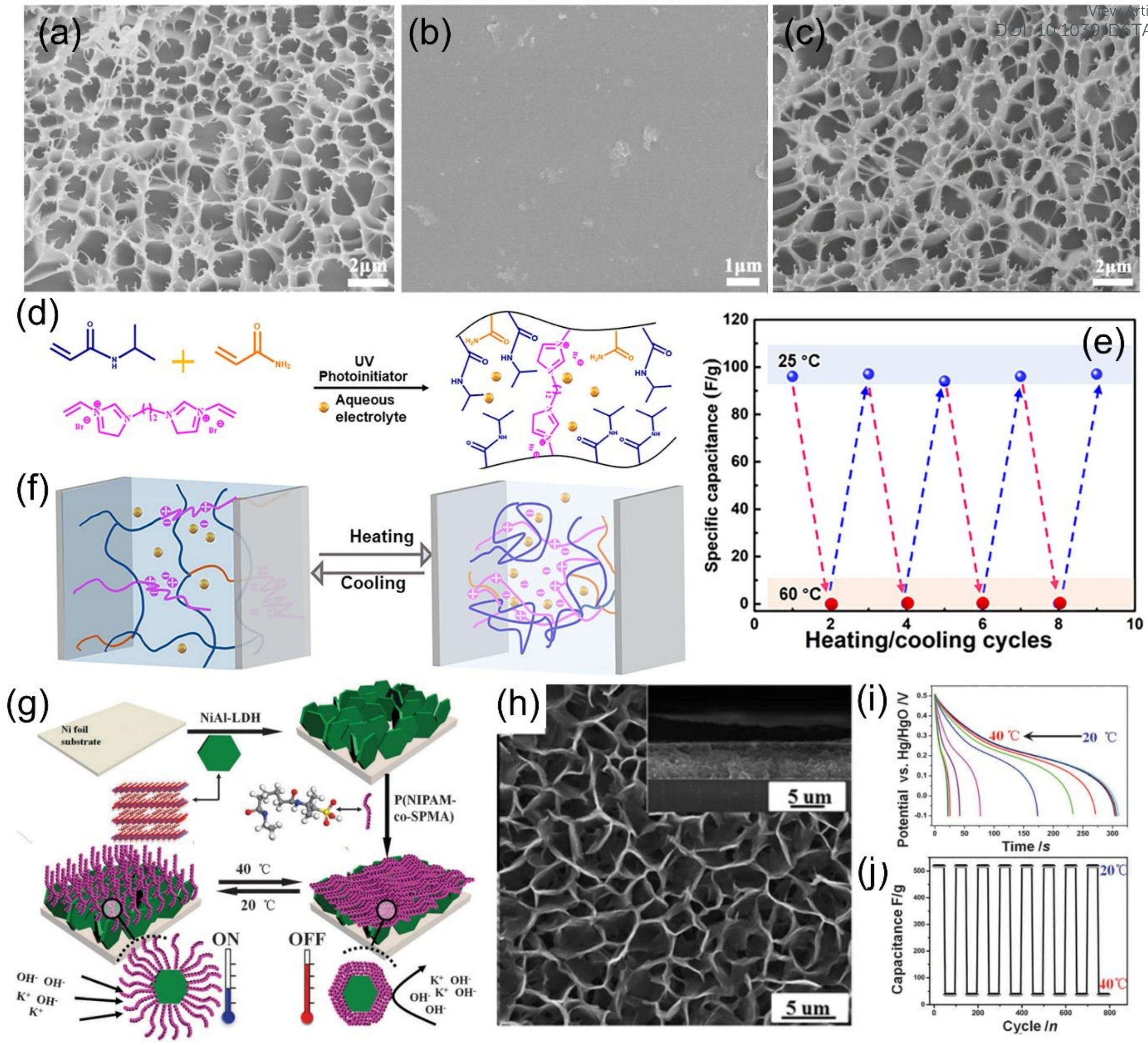

Figure 3. Morphologies of PNIPAM/NMAM under heating/cooling cycles: (a) 25 °C, (b) 70 °C, and (c) 25 °C (cooling down), respectively.[22] Reproduced with permission.[22] Copyright 2021, American Chemical Society. (d) Illustration of preparation of PNIPAM hydrogels through in-situ polymerization. (e) Repeatable capacitances of SCs based on the PNIPAM hydrogel and (f) corresponding illustration of ion migrations under heating/cooling cycles.[79] Reproduced with permission.[79] Copyright 2023, American Chemical Society. (g) Illustration of the preparation of LDH@P(NIPAM-co-SPMA) film electrode and its working principle towards thermally-response. (h) SEM images of the LDH@P(NIPAM-co-SPMA) film. (i) Discharge curves of LDH@P(NIPAM-co-SPMA) film electrode under different temperature and (j) its corresponding specific capacitance upon the cooling/heating process.[27] Reproduced with permission.[27] Copyright 2013, Royal Society of Chemistry.

3.1.2 PEO/PPO-based polymers for temperature-responsive SCs

Although the above-mentioned PNIPAM polymer-based electrolytes can be used to construct the temperature-responsive SCs, poor interfacial compatibility between the electrolyte and the electrode surface, slow response rate, and relatively low LCST negatively affected the overall capacitive performance and limited the operation temperature range of the obtained SCs as well as their practical applications. Therefore, it was necessary to explore new electrolyte systems for further improvement. Among them, devices using PEO/PPO-based polymers have shown great promise for electrolytes in the design of temperature-responsive SCs. PEO was a crucial component in creating thermoresponsive polymers, especially when combined with hydrophobic blocks like PPO, which can produce materials with tunable LCST and be used to construct temperature-responsive SCs. A representative example of such an electrolyte system was the PEO/1-ethyl-3-methylimidazolium tetrafluoroborate ([EMIM][BF_4]) composite electrolyte (**Figure 4a**),[12] which was comprised of an ionic liquid (IL) (here, IL refers to [EMIM][BF_4]), PEO, and Li^+ salts. As shown in **Figure 4b**, the increment of charge storage of the SCs based on active carbon (AC) electrodes in pure [EMIM][BF_4] electrolyte was proportional to the working temperature. However, noted that its capacitance at 160 °C dropped approximately 30 % compared to the value at 100 °C (**Figure 4c**). These electrochemical results revealed that the L-PEO–[EMIM][BF_4] electrolyte impeded electrochemical processes at elevated temperature because of a thermally activated phase separation in the L-PEO–[EMIM][BF_4] (50/50) electrolytes above 140 °C. Briefly, when the working temperature was above 140 °C, a PEO-rich phase was formed inside the nanopores of AC, which hindered charge accumulation at the electrode/electrolyte interface, thus leading to the decay of storage charge. Therefore, the smart responsive polymer electrolyte system showed promise for further development of thermos-responsive SCs.

Inspired by this work, Pluronic copolymer, which was a triblock copolymer with a central hydrophobic chain of PPO flanked by two hydrophilic chains of PEO, forming a PEO-PPO-PEO structure, was synthesized,[28] making it amphiphilic. The unique structure of Pluronic copolymer can self-assemble in water into micelles and change from liquid to gel with increasing temperature (**Figure 4d**), thus making it more attractive for the design of thermoresponsive SCs. According to the results in **Figure 4e**, the device exhibited a relatively high specific capacitance at 20 °C, but its capacitance dropped by approximately 50% at 70 °C (**Figure 4f**), which was due to the electrolyte gelation. Furthermore, by adjusting the concentration of the Pluronic solution from 30 wt% to 5 wt%, the transition temperature can be regulated over a wide range. This was because, when the Pluronic solution concentration decreased, the average distance between micelles became larger. In this case, a higher temperature was required to derive the polymer chains to become fully entangled. In addition, the capacity loss can be controlled by the molecular weights of Pluronic solutions. These

View Article Online
DOI: 10.1039/D6TA00650G

adjustable properties made this electrolyte a promising candidate for the construction of smart SCs.

Due to the attractive chemical/physical properties of Pluronic polymer mentioned above, it was extended to explore other non-aqueous smart electrolytes and then construct smart SCs. For instance, a thermal-responsive electrolyte consisting of [EMIM][BF_4], Pluronic F127 (PEO-b-PPO-b-PEO), and lithium tetrafluoroborate ($LiBF_4$) was successfully prepared.[80] Compared with the pure $LiBF_4$ electrolyte system, the Pluronic-IL electrolyte system exhibited significantly temperature-dependent electrochemical performance (**Figure 4g, 4h**). The SCs in a 20 wt% Pluronic-IL electrolyte delivered a capacitance of 40 $F \cdot g^{-1}$ at 100 °C, while it only maintained about 17.6 $F \cdot g^{-1}$ at 160 °C (a 56% loss in specific capacitance), which indicated that ion migration was significantly suppressed at high temperatures. This temperature-dependent capacitance variation was attributed to the compositional structure of Pluronic-[EMIM][BF_4] (**Figure 4i**), which controlled the resistance of ion migration. In this structure, the PEO segment was [EMIM][BF_4]-philic due to hydrogen bonds formed between the epoxy groups and the C2-H of the imidazole cations, and between the BF^- and H^- at the Pluronic hydroxyl terminus. Furthermore, the PPO segment was [EMIM][BF_4]-phobic, leading to micelle formation, allowing Pluronic to be well dispersed in [EMIM][BF_4] and move freely below the transition temperature. However, above the transition temperature (≥130°C), the hydrogen bonds between the PEO segments and the ionic liquid weaken, and the PEO segments became entangled, forming a gel electrolyte. The highly reversible sol-gel transition behavior of Pluronic-[EMIM][BF_4] electrolytes enabled the design of energy storage devices with smart thermos-responsive property.

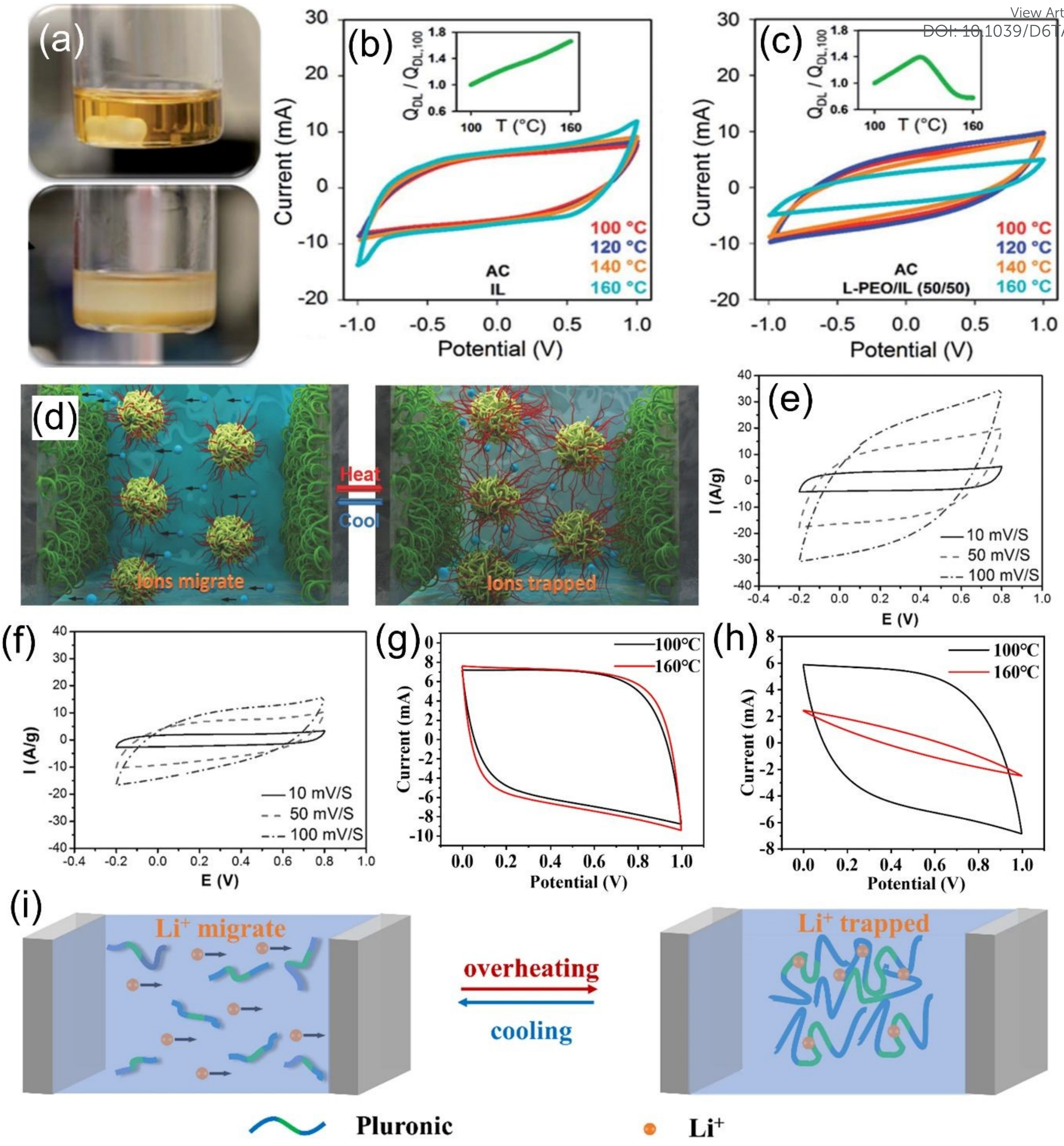

Figure 4. (a) Photographs of the PEO/[EMIM][BF$_4$] mixture electrolyte at room temperature (Up) and high temperature (Down). Temperature dependence of CV profiles for AC electrodes in (b) pure [EMIM][BF$_4$] and (c) L-PEO/[EMIM][BF$_4$] (50/50) electrolytes under different testing temperatures.[12] Reproduced with permission.[12] Copyright 2015, Royal Society of Chemistry. (d) Illustration of the obtained gel electrolyte under heating/cooling cycles. The CV curves of the device using 20 wt% Pluronic solution (MW ≈ 5800 Da) dissolved with aqueous H_2SO_4 as the electrolyte at (e) 20 °C and (f) 70 °C, respectively.[28] Reproduced with permission.[28] Copyright 2016, Wiley-VCH. CV curves at 100 mV·s^{-1} for (g) pure [EMIM]BF$_4$ and (h) Pluronic-[EMIM]BF$_4$ electrolytes with 0.01 M LiBF$_4$. (i) Illustration of the Pluronic-IL electrolyte under heating/cooling cycles.[80] Reproduced with permission. [80] Copyright 2022, Springer Nature.

3.1.3 Cellulose derivatives for temperature-responsive SCs

View Article Online
DOI: 10.1039/D6TA00650G

Clearly, the strategy of constructing temperature-responsive smart SCs through the rational design of polymer electrolytes was promising. Typically, thermoresponsive electrolytes (e.g., PNIPAM-based polymers, PEO/PPO-based polymers) underwent sol-gel transition/phase separation at high temperature,[37] which suppressed ion migration and reduced ionic conductivity, thus resulting in temperature-dependent capacitor behavior in the SCs. However, these copolymers still displayed some drawbacks. For instance, PNIPAM-based polymers were commonly used in the design of smart SCs but were mostly limited to copolymers of NIPAM with AA or AM.[11, 26, 81] Furthermore, their properties were often affected by the pH of electrolyte. In addition, for the reported Pluronic electrolytes, the use of high concentration not only increased the overall cost but also compromised the electrochemical performance.[28, 37]

Considering the drawbacks mentioned above, it was necessary to explore alternative thermoresponsive electrolytes. Among them, cellulose-based derivatives have attracted attention due to their relatively high LCST and high sensitivity to temperature changes. As a representative example, a cellulose-derivative electrolyte was prepared by dissolving MC in aqueous H_2SO_4 solution (**Figure 5a**).[42] Noted that the capacitance of AC electrode was about 90 $F\cdot g^{-1}$ in MC/H_2SO_4 electrolyte at 25 °C while reducing to 9 $F\cdot g^{-1}$ at 70 °C and then returning 90 $F\cdot g^{-1}$ after cooling down (**Figure 5b**). The thermal switching capacitive behavior was attributed to the adjustable ion transport of this cellulose-derivative electrolyte during the heating/cooling cycles.[42, 77] Subsequently, to further optimize the application of cellulosic electrolytes in smart SCs, MC-g-PEO copolymer electrolytes were synthesized by the same research group using a free radical copolymerization method (**Figure 5c**).[43] Notably, the resulting microsupercapacitors (MSCs) completely lost its capacitance at 80 °C while recovering to its initial value at 25 °C (**Figure 5d**). The reversible thermoresponsive electrochemical performance of MSCs was due to the phase transition of MC-g-PEO copolymer electrolytes during heating and cooling cycles (**Figure 5e**). In short, when the temperature was above LCST, a gelation process occurred, which effectively inhibited ion migration, leading to a decrease of the capacitance of the MSCs. However, at room temperature, the electrolyte transformed to a solution state, allowing the electrolyte ions to migrate freely. The superior performance of MSCs based on MC-g-PEO thermoresponsive copolymer electrolyte provided a promising strategy for the design of smart thermoresponsive SCs and other portable microelectronic devices.[43, 77] Based on the aforementioned literature and related analysis, thermoresponsive polymers can serve as a “thermal gating”, resulting in a reversible switch-off/on of capacitor behavior upon heating/cooling. This reversible temperature-

View Article Online
DOI: 10.1039/D6TA00650G

triggered capacitor behavior (**Table 2**) made them ideal materials for designing thermoresponsive smart SCs.

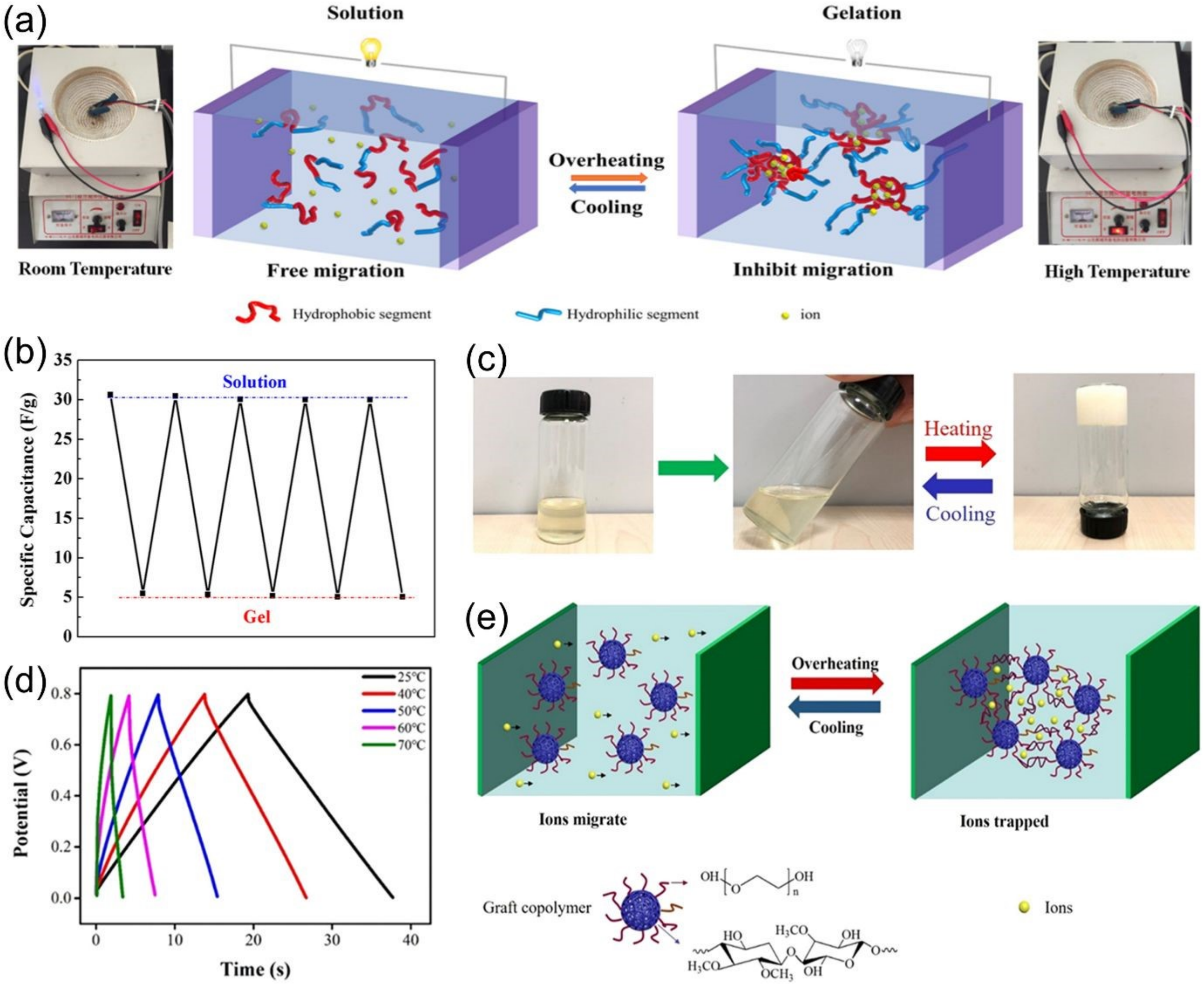

Figure 5. (a) Illustration of the MC/H_2SO_4 electrolyte with reversible thermoresponsive properties as well as the digital photographs of the LED powered by the home-made SCs based on the MC/H_2SO_4 electrolyte. (b) Capacitance of SCs based on the MC/H_2SO_4 electrolyte cycling between 25 °C and 70 °C.[42] Reproduced with permission.[42] Copyright 2018, American Chemical Society. (c) Photographs of the states of the MC-g-PEO copolymer electrolyte under heating/cooling cycles. (d) Charge/discharge curves of MSCs at 1 $A \cdot g^{-1}$. (e) Illustration of the phase transition of the MC-g-PEO copolymer electrolyte during the heating/cooling cycles.[43] Reproduced with permission.[43] Copyright 2019, American Chemical Society.

Table 2. Electrochemical performance comparison of temperature-responsive SCs.

Electrolyte	**Potential window (V)**	**Capacitance (F·g^{-1})**		**Ref.**
		Low temperature	**High temperature**	
PNIPAM-AA copolymer	0-0.7	N.A. (20 ℃)	85% capacitance loss (50 ℃)	[11]
LiOH-PNIPAM/AM	0-0.8	52.5 (20 ℃)	34.0 (70 ℃)	[26]
P(NIPAM-co-GMA)/H_2SO_4	-0.35-0.2	118 (20 ℃)	51.9 (85 ℃)	[37]
PNIPAM-co-NMAM/LiTFSI	0-0.6	242.8 mF·cm^{-2} (25 ℃)	34 mF·cm^{-2} (70 ℃)	[22]
PEO-[EMIM][BF_4]-$LiBF_4$	-1.0-1.0	N.A. (100 ℃)	70% capacitance loss (160 ℃)	[12]
Pluronic solution/H_2SO_4	-0.2-0.8	110 (20 ℃)	10 (70 ℃)	[28]
Pluronic-[EMIM][BF_4]-$LiBF_4$	0-1.0	40 (100 ℃)	17.4 (140 ℃)	[80]
MC/H_2SO_4 electrolyte	-0.2-0.8	90 (25 ℃)	9 (70 ℃)	[42]
MC-g-PEO copolymer	0-0.8	59.5 (25 ℃)	0 (80 ℃)	[43]

View Article Online
DOI: 10.1039/D6TA00650G

3.2. Magnetic-responsive SCs

As mentioned earlier, the advantages of magnetic field-induced magnetization were crucial for the design of magnetic-responsive SCs. Generally, ferromagnetic materials retained their magnetization, while paramagnetic materials lost their magnetism upon removal of the applied magnetic field. Therefore, the interaction between paramagnetic materials and the applied magnetic field provided the opportunity for the design of magnetic-responsive-based SCs.[82] Currently, there are two main strategies for boosting the electrochemical performances of electrodes through external magnetic interactions: (a) integrating magnetic nanoparticles into electrodes; (b) reconstructing charge density and electric polarization. Despite considerable efforts, it was essential to systematically summarize this relevant research to better understand the origin of magnetic field-dependent supercapacitive properties, thus providing useful guidance for the design of magnetic-responsive smart SCs.

3.2.1 Metal oxides for magnetic-responsive SCs

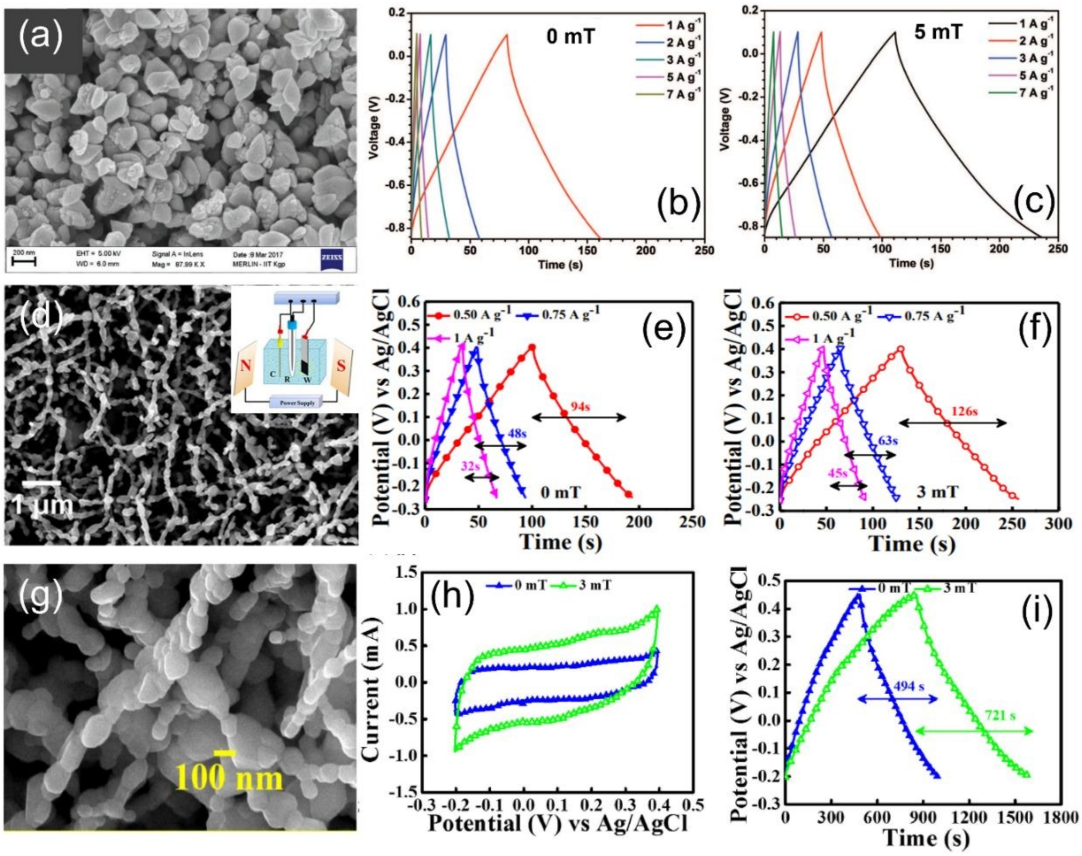

Figure 6. (a) SEM image of nanoleaflet-like Fe_2O_3. Charge/discharge curves in the (b) absence and (c) presence of magnetic field, respectively.[13] Reproduced with permission.[13] Copyright 2018, Wiley-VCH. (d) SEM image of the sintered $FeCo_2O_4$ nanofibers and its corresponding charge/discharge curves in the (e) absence and (f) presence of magnetic field, respectively.[83] Reproduced with permission.[83] Copyright 2020, American Chemical Society. (g) SEM image

View Article Online
DOI: 10.1039/D6TA00650G

of the sintered $FeMn_{0.2}Co_{1.8}O_4$ nanofibers and its corresponding (h) CV curves and (i) charge/discharge curves with and without of magnetic field, respectively.[87] Reproduced with permission.[87] Copyright 2021, Elsevier.

Among transition metal oxides, magnetic metal oxides (e.g., Fe_2O_3, Mn_3O_4, $FeCo_2O_4$), have attracted great attention. It was reported that the effect of the magnetic field on the performance of the electrode materials was closely related to their properties (e.g., magnetism, conductivity) and microstructure (e.g., crystal structure, surface area, pore size).[83] Therefore, it can be expected that magnetic metal oxides with unique magnetic properties and microstructures will exhibit a significant discrepancy in the capacitor behavior of SCs in the absence and presence of magnetic field. Regarding magnetic metal oxide, Fe_2O_3 was widely used as the electrode material for the design of magnetic-responsive SCs. As a proof-of-concept, 2D nanoleaflet-like Fe_2O_3 was synthesized by refluxing at 95 °C for 12 h followed by heat-treatment in air (**Figure 6a**).[13] The electrochemical performance of the 2D nanoleaflet-like Fe_2O_3 was investigated in three-electrode system. Noted that nearly 61% increase in the specific capacitance, a 170% increase in energy density, and a ten-fold increase in power density were observed under a magnetic field compared with the counterpart without a magnetic field (**Figure 6b, 6c**). These results clearly showed that its capacitor behavior was enhanced under a magnetic field, which was attributed to the changes in the thickness of the Nernst layer and reduction in charge transfer resistance.[13]

Like other typical magnetic metal oxides, Mn_3O_4 has also attracted great attention due to its mixed valence states and distinct crystal structure. Interestingly, a very recent study revealed that Mn_3O_4 showed an opposite magnetic field-dependent variation of specific capacitance when applying a magnetic field. This observation seemed to be contrary to other magnetic metal oxides. A question arose about the reason for this unusual phenomenon of the Mn_3O_4 electrode for SCs under a magnetic field. It is noted that compared with MnO_2 and other common metal oxides, Mn_3O_4 showed an increased dielectric constant under a magnetic field, indicating enhanced insulation property. This led to a decrease in total charge collection efficiency and specific capacitance during device operation.[84]

Moreover, the energy storage performance of metal oxides was closely related to surface area, shape, and size.[29, 85] Therefore, controlling surface area, shape, and pore size was an effective strategy for boosting the capacitor behavior of electrode materials. Particularly, metal oxide nanofiber with one-dimensional, high aspect ratio, and porous structure was considered

View Article Online
DOI: 10.1039/D6TA00650G

as an attractive material.[83, 86] In this context, $FeCo_2O_4$ nanofibers were fabricated by the electrospinning technique (**Figure 6d**).[83] Notably, after applying a magnetic field (3 mT), the capacitance of the $FeCo_2O_4$ nanofibers increased about 34% at 0.5 $A\cdot g^{-1}$ (**Figure 6e, 6f**). The performance improvement was primarily attributed to the effect of the magnetic field on its bulk resistance and magnetoresistance. Clearly, the applied magnetic field enhanced the overall effective field acting on the local spin and reduced spin fluctuations, thereby reducing electron-spin scattering and ultimately leading to a decrease of bulk resistance of the $FeCo_2O_4$ nanofibers. Additionally, both Lorentz force and magnetic gradient force acted simultaneously and played a crucial role in regulating ion/electron movement during charging and discharging processes.[83]

Furthermore, doping of suitable metal elements into spinel-structured ferrites was proved to change their magnetism. Thus, an identical approach was used to improve the capacitance values of the given material. Knowing this, the same group doped Mn element into $FeCo_2O_4$ nanofibers (**Figure 6g**).[87] The capacitor behavior of Mn-doped $FeCo_2O_4$ nanofiber electrode was studied with and without a magnetic field. The specific capacitance of $FeMn_{0.2}Co_{1.8}O_4$ at 3 $mV\cdot s^{-1}$ was 306 $F\cdot g^{-1}$ under a magnetic field (Figure 6h), which was much higher than that of the $FeMn_{0.2}Co_{1.8}O_4$ electrode (212 $F\cdot g^{-1}$) without a magnetic field. Surprisingly, a 46% capacitance increment was observed for the $FeMn_{0.2}Co_{1.8}O_4$ electrode under a magnetic field (3 mT) based on the charge/discharge curves (**Figure 6i**), which were consistent with the results of CV curves. The excellent performance of the $FeMn_{0.2}Co_{1.8}O_4$ electrode under an external magnetic environment was mainly due to the increment of the conductivity induced by Mn doping and the gradient force created by the magnetic susceptibility. The doping of Mn into the $FeCo_2O_4$ can lower its internal resistance, while the induced gradient force can reduce the thickness of the Nernst layer and favor the ion and electronic transport at the electrode/electrolyte interface. This study showed a novel strategy for improving the capacitor behavior of electrode material by doping appropriate elements and applying an external magnetic field.[87]

3.2.2 Nanocomposites for magnetic-responsive SCs

Magnetic metal oxides were promising electrode materials for SCs due to their high pseudocapacitance but often suffered from unsatisfactory power density and poor cycling stability. As an alternative strategy, composite materials were popularly used as electrode materials for SCs. This is because the high conductivity and stability of one material, combined

View Article Online
DOI: 10.1039/D6TA00650G

with the high capacitance value of another, created a synergetic effect, thus improving electrochemical performance.[88] From this perspective, researchers tried to boost their performance by preparing nanocomposites, which typically involved the magnetic metal oxides incorporated with conductive polymers or different types of carbon materials, thus achieving a trade-off between high capacitance and good cycle stability. In this sense, coupling the magnetic metal oxides with conductive polymers was a feasible strategy to overcome the above-mentioned issues and achieve enhanced performance. Fe_3O_4/PPy nanocomposites were fabricated *via* a simple surface-initiated polymerization method.[89] The Fe_3O_4/PPy nanocomposite displayed the enhancement of capacitive behavior. Particularly, under a magnetic field, its energy density was 10 times higher than that of its counterparts without a magnetic field. With a magnetic field, the movement of the electrolyte ions was accelerated by an extra Lorentz force. Undoubtedly, with a magnetic field, faster-moving ions can more efficiently compensate for the ions consumed in redox reactions, thus contributing to electrochemical performance improvement.[89]

Recently, the combination of advanced carbon materials with magnetic metal oxides has also attracted considerable interest.[90, 91] For instance, MnO_2/carbon nanofiber composite was fabricated by electrospinning followed by electrochemical deposition (**Figure 7a-7d**).[92] The electrochemical performance of MnO_2/carbon nanofiber composite with and without magnetic field was investigated (**Figure 7e**). With an applied magnetic field, the MnO_2/carbon nanofibers showed the magneto-enhanced performance in terms of higher charge density, longer discharge time and lower internal resistance, indicating the magneto-enhanced capacitor performance. The enhancement was attributed to the fast electron transfer reaction arising from the magnetic susceptibility of MnO_2 induced electron spin, the fast mass transport, and the improved cation intercalation/de-intercalation.[92] As another representative example, AC/Fe_3O_4 nanocomposite was synthesized *via* a simple hydrothermal method followed by ultrasonication.[93] Its electrochemical performance was investigated under magnetization and non-magnetization conditions, respectively. Encouragingly, the capacitor behavior of AC/Fe_3O_4 nanocomposite was boosted with the implementation of a magnetic field, which was due to the magnetic field improving ion/electron transport and reducing charge transfer resistance. Specifically, under the magnetization conditions, the introduction of Lorentz force improved the transportation efficiency of the electrons, and the change in the microscopic structure of the electrolyte molecules enhanced the electrical conductivity of the electrolyte, thus contributing to the improvement of supercapacitive performance.[93] Similarly,

View Article Online
DOI: 10.1039/D5TA00650G

graphene/Fe_2O_3 nanocomposite was fabricated by a facile thermal decomposition (**Figure 7f**).[91] Noted that the graphene/Fe_2O_3 nanocomposite electrode showed 92.5% specific capacitance enhancement in the presence of a magnetic field (**Figure 7g, 7h**). Moreover, the corresponding energy and power densities were also enhanced in the presence of a magnetic field, which was attributed to the significant restriction of the interfacial relaxation process. This work presented a new and effective strategy for improving the capacitor behavior under a magnetic field and for constructing magnetic-responsive SCs.[91]

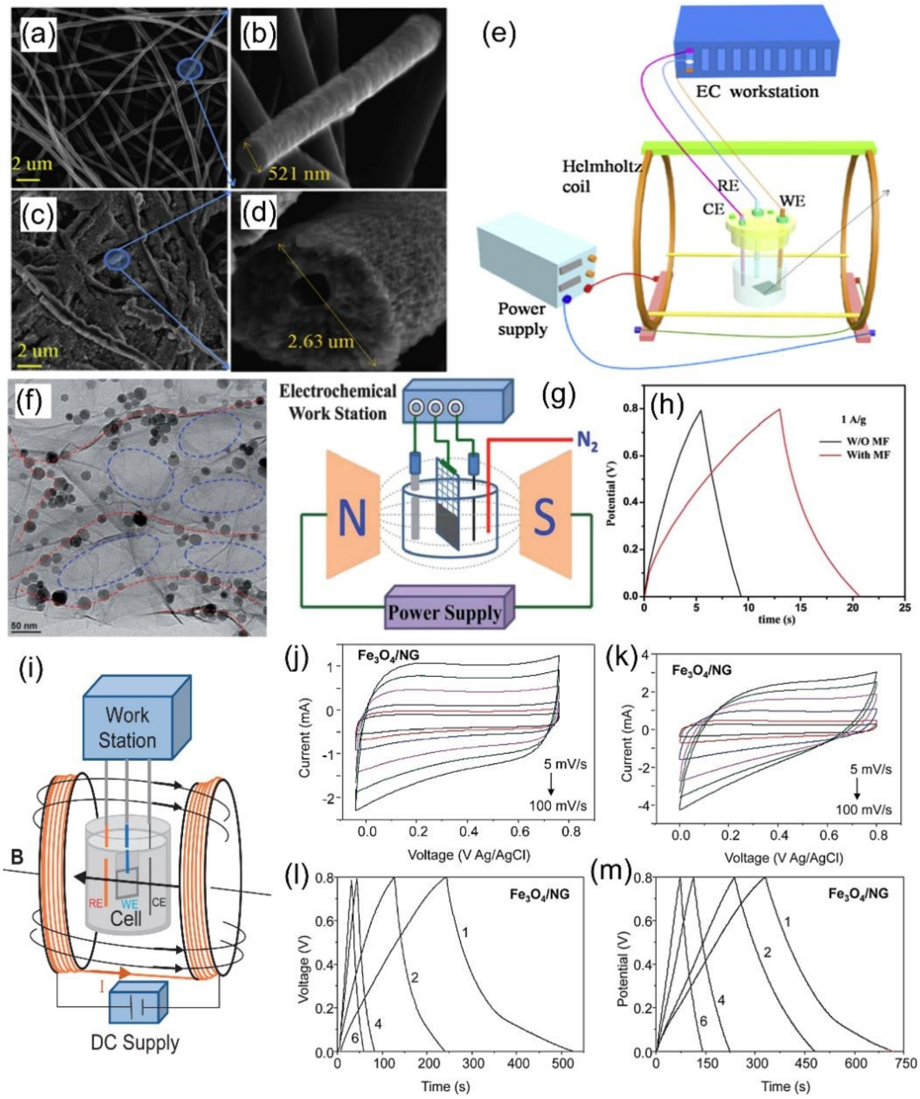

Figure 7. SEM images of (a, b) pure carbon fiber and (c, d) MnO_2/carbon fiber, respectively. (e) Illustration of the electrochemical setup for MnO_2/carbon fiber electrode tested under an external magnetic field.[92] Reproduced with permission.[92] Copyright 2017, Elsevier. (f) TEM image of graphene/Fe_2O_3 nanocomposites. (g) Illustration of the capacitor behavior of graphene/Fe_2O_3 tested in a magnetic field and (h) corresponding charge/discharge curve.[91] Reproduced with permission.[91] Copyright 2013, Royal Society of Chemistry. (i) Schematic diagram of the electrochemical performance of Fe_3O_4/nitrogen-doped graphene conducted in the presence of external magnetic field. (j, k) CV curves and (l, m) charge/discharge curves of

View Article Online
DOI: 10.1039/D6TA00650G

the Fe_3O_4/nitrogen-doped graphene with and without of a magnetic field.[94] Reproduced with permission.[94] Copyright 2020, Oxford University Press.

Up to now, many efforts have been made to design magnetic metal oxide-based electrodes, which displayed obvious magnetic-induced capacitor behavior. However, it was still a great challenge to explore a simple and universal strategy for the synthesis of magnetic metal oxides with significant enhancement of capacitor behavior. Taking this into account, a general approach was proposed to synthesize magnetic metal oxide-based hybrid materials. A series of metal oxides (e.g., NiO, Co_3O_4, and Fe_3O_4)/nitrogen-doped graphene (NG) composites were synthesized by in-situ deposition of magnetic metal oxides on nitrogen-doped graphene.[94] The electrochemical performance of these hybrid electrodes was evaluated without and with an external magnetic field. Here, taking Fe_3O_4/nitrogen-doped graphene (Fe_3O_4/NG) as example, the effect of an applied magnetic field on the capacitor behavior was investigated (**Figure 7i**). The results showed that the capacitance of Fe_3O_4/NG increased about 28.8% after applying a magnetic field compared to the state without a magnetic field (**Figure 7j, 7k**). Furthermore, Fe_3O_4/NG also exhibited a longer discharge time with a magnetic field compared to its counterpart (**Figure 7l, 7m**), indicating improved performance, consistent with the results of CV curves. These electrochemical results demonstrated that the magnetic field played a crucial role in the charge/discharge process of the Fe_3O_4/NG electrode. Clearly, the magnetic field significantly enhanced the charge carrier transportation through the Lorentz force, thus promoting electrolyte convection and enhancing ion transport. In addition, the magnetic field can reduce the interfacial resistance by decreasing charge transfer resistance and increasing the charge transport efficiency between the electrode and the electrolyte. In a word, the improved ion transport, the increased interface charge density, and the reduced resistance enhanced the capacitor behavior.[94]

According to the above discussion, the electrochemical performance of SCs can be effectively regulated by a magnetic field (**Table 3**). In short, the capacitor behavior of the electrode materials was improved with a magnetic field due to the increase of electron transportation efficiency. Furthermore, the Lorentz force acted on moving charges/ions in the electrolyte and led to the electrolyte ions to move in a circular pattern towards the electrode surface, thereby causing the electrolyte convection and reducing the resistance of the bulk electrolyte. Meanwhile, this magnetohydrodynamic effect pushed the electrolyte ions to reach extra electrode surface area, which can not be accessed without applying the magnetic field. In

View Article Online
DOI: 10.1039/D5TA00650G

a word, the tunable capacitor behavior under the magnetic field could be a promising strategy for the design of magnetic-responsive SCs.

Table 3. Electrochemical performance comparison of magnetic-responsive SCs.

Electrode material	**Electrolyte**	**Potential window (V)**	**Capacitance (F·g^{-1})**		**Ref.**
			Without magnetic field	**With magnetic field**	
2D nanoleaflet-like Fe_2O_3	1 M KOH	-0.85-0.1	86 (1 A ·g^{-1})	134 (1 A ·g^{-1})	[13]
Mn_3O_4	1 M Na_2SO_4	0-1.0	208 (1 A ·g^{-1})	156 (1 A ·g^{-1})	[84]
$FeCo_2O_4$ nanofibers	2 M KOH	-0.25-0.4	106 (3 mV·s^{-1})	165 (3 mV·s^{-1})	[83]
$FeMn_{0.2}Co_{1.8}O_4$	2 M KOH	0-0.6	212 (3 mV·s^{-1})	306 (3 mV·s^{-1})	[87]
Fe_3O_4/PPy nanocomposite	1 M H_2SO_4	-1.2-0.8	332.9 (1 A ·g^{-1})	413.8 (1 A ·g^{-1})	[89]
MnO_2/carbon nanofiber composite	6 M KOH	0-0.8	114 (1 A ·g^{-1})	180 (1 A ·g^{-1})	[92]
AC/Fe_3O_4 nanocomposite	6 M KOH	-1.0-0	136 (1 A ·g^{-1})	105 (1 A ·g^{-1})	[93]
Graphene/Fe_2O_3 nanocomposite	1 M Na_2SO_4	-1.0-1	208 (1 A ·g^{-1})	156 (1 A ·g^{-1})	[91]
Fe_3O_4/nitrogen-doped graphene	1 M NaCl	0-0.8	5.4 (1 A·g^{-1})	8.6 (1 A·g^{-1})	[94]

View Article Online
DOI: 10.1039/D6TA00650G

3.3 Photo-responsive SCs

Photo-responsive SCs were another new type of smart SCs, in which the incorporation of electrode materials with light-responsive properties gave the resulting SCs with photo-responsive characteristics and enhanced capacitor behavior. In this device, the photoactive materials (e.g., conducting polymers, metal sulfides, metal oxides) absorbed light to generate electron-hole pairs,[95] which then drove the fast surface redox reaction or formed the double-layer capacitor. Therefore, the development of optically light-driven SCs required electrode materials that enabled both photogenerated electrons and holes to be internally separated. Undoubtedly, the rational design and construction of the light-responsive electrodes were one of the important factors to achieve the excellent capacitor performance.

3.3.1 Conducting polymers for photo-responsive SCs

Currently, scientists have made many efforts to explore novel photo-responsive positive electrodes (e.g., conducting polymers, metal sulfides, metal oxides). Particularly, by using different synthesis methods to design and prepare the photo-responsive materials with controllable morphology and structure, the as-prepared SCs exhibited good photo-responsiveness and light-enhanced supercapacitive behavior. Among these developed photo-responsive electrodes, conducting polymers with an extended π-electron system in their backbone have attracted tremendous attention. Conducting polymer photoresponsive electrodes offered several advantages for photo-enhanced SCs (e.g., narrower bandgaps, high charge carrier mobility, tunable electrical properties). Furthermore, the electrical and optical properties of conducting polymers can be tuned by adjusting the synthesis methods, optimizing the parameters, and forming composites with other nanomaterials. Additionally, the conducting polymers possessed inherent flexibility, lightweight, and low cost, making them attractive candidates for wearable SCs.

Regarding these reported polymers, boron-dipyrromethene (BODIPY) and their derivatives were widely used in many fields (e.g., optoelectronics, photocatalysis, molecular sensing) due to their exceptional photophysical and chemical properties.[96] Recently, it has caused growing interest in incorporating BODIPY into redox-active porous frameworks to simultaneously harvest the light energy and store the charge. Here, a cross-linked thieno [3,2-b] thiophene-BODIPY porous polymer, synthesized by using the thiol-ene click chemistry method (**Figure 8a, 8b**), was employed as the electroactive material for the design of light-responsive SCs (**Figure 8c**).[14] The extended conjugation in this BODIPY-derived porous polymer not only

View Article Online
DOI: 10.1039/D6TA00650G

possessed a broad absorption spectrum, but also enabled a low optical bandgap, thereby facilitating the light harvesting and charge transport. Obviously, there was a significant growth of discharge time (**Figure 8d**) and specific capacitance (**Figure 8e**) under visible light illumination, attributed to the good photo-induced charge separation and enhanced carrier mobility. Moreover, the BODIPY-derived polymer electrode also exhibited remarkable cycle stability with about 90% capacitance retention after 2000 cycles under the light illumination (**Figure 8f**), indicating its robust structural stability. The unique framework structure along with remarkable physicochemical properties enabled the BODIPY-derived porous polymer to improve the chemical stability and favor efficient photoinduced charge transport under illumination, thus boosting the capacitor behavior.[14]

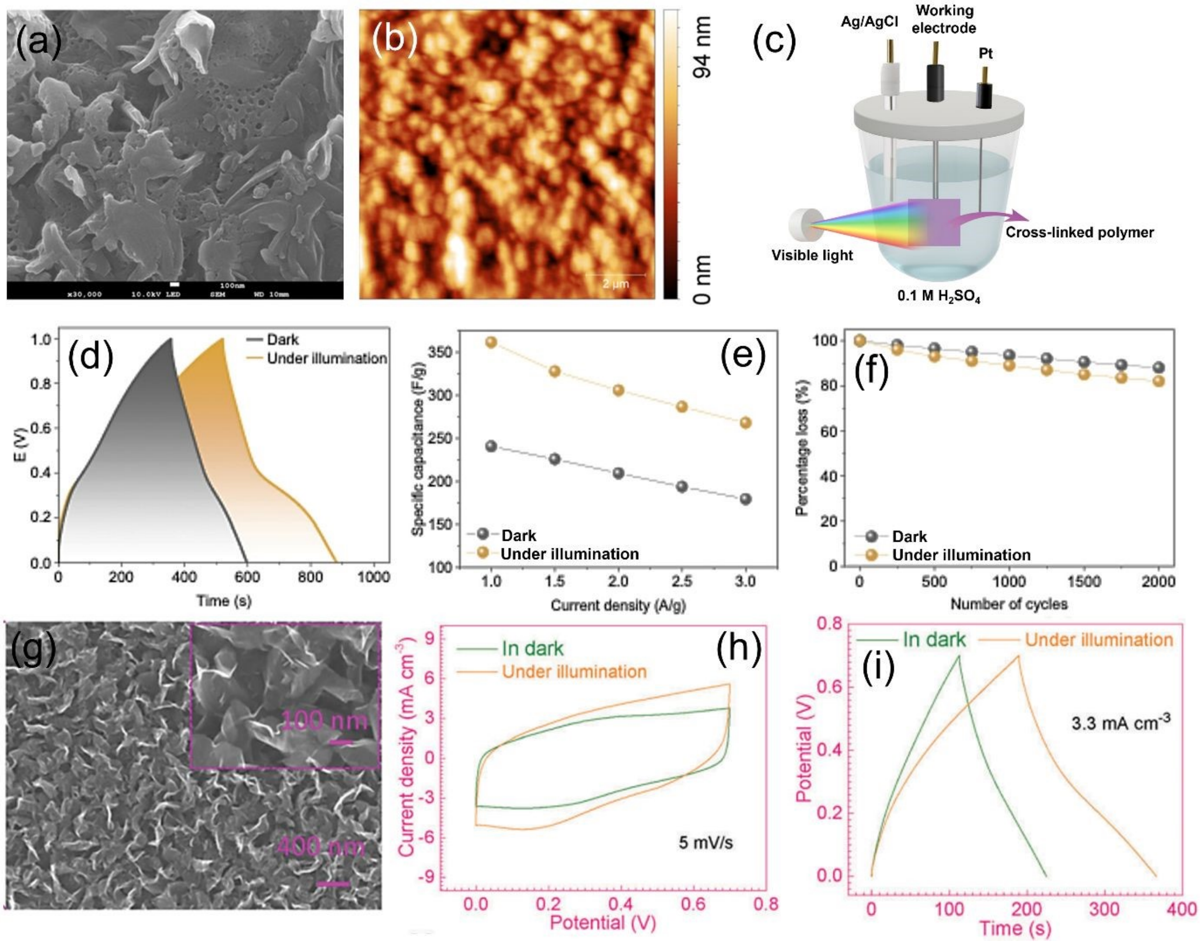

Figure 8. (a) SEM and (b) AFM images of BODIPY-derived porous polymer. (c) Photo-assisted three-electrode electrochemical cell configuration and its corresponding (d) charge–discharge curves, (e) specific capacitance under different current densities, and (f) cycle stability.[14] Reproduced with permission.[14] Copyright 2025, American Chemical Society. (g) SEM images of the 3D-graphene support. (h) CV curves and (i) charge/discharge curves of the SCs-based on 3D-graphene coated PEDOT:PSS electrode in the dark and under illumination.[98] Reproduced with permission.[98] Copyright 2018, Royal Society of Chemistry.

View Article Online
DOI: 10.1039/D5TA00650G

Lately, the same group used a similar thiol-ene click reaction method to cross–link donor–acceptor building blocks on a graphene sheet substrate,[97] thus enabling the resulting porous organic polymer for electrode materials of the photo-responsive SCs. This photoactive polymer electrode showed a capacitance of 304.1 $F\cdot g^{-1}$ (at 2.0 $A\cdot g^{-1}$) and an energy density of 60 $Wh\cdot kg^{-1}$ under visible light, which was almost two times higher than that under dark conditions. Meanwhile, the obtained polymer electrode exhibited excellent cycling stability. The remarkable performance of the photoactive polymer presented here revealed that combining donor–acceptor engineering with thiol–ene click reaction was an effective strategy for constructing photo-assisted SCs with improved electrochemical performance.[97]

However, pure conducting polymer electrode suffered from some drawbacks, such as unsatisfactory stability, relatively low electronic conductivity, and poor electron-hole separation. Therefore, the design of conducting polymer composite was considered as another effective strategy to enhance the capacitor behavior. For instance, a photoresponsive pseudo-capacitor was assembled with 3D graphene (**Figure 8g**) coated with a PEDOT:PSS electrode.[98] Interestingly, compared with the device tested in the dark, the device displayed a larger area surrounded by the CV curve (**Figure 8h**), a longer discharge time (**Figure 8i**), and a larger volumetric capacitance, demonstrating a significant improvement in capacitor performance under solar illumination. Noted that the enhancement of the capacitor behavior of the device under illumination was due to the photo-induced effect, which increased the electrode conductivity and the reaction rate constant. In addition, the strategy can be extended to other materials with high light thermal conversion efficiency.[98]

3.3.2 Metal sulfides for photo-responsive SCs

Owing to their intermediate to narrow band gaps, good electrical conductivity, high ionic diffusivity, and high specific capacitance, metal sulfides were also considered as excellent pseudocapacitive candidates for the construction of photo-responsive SCs. As an example, a light-induced SCs was built with vertically aligned ReS_2 nanosheets grown on conducting substrates *via* chemical vapor deposition (**Figure 9a**).[30] Vertically aligned ReS_2 nanosheet electrode (**Figure 9b**) showed a larger area enclosed by the CV curve than the counterpart (**Figure 9c**), demonstrating an increased charge storage under light illumination. Also, the ReS_2 nanosheet electrode possessed a longer discharge time and a higher volumetric capacitance under a series of current densities with the presence of light (**Figure 9d**). The supercapacitive performance enhancement was due to the generated electron-hole pairs under light illumination

View Article Online
DOI: 10.1039/D6TA00650G

(**Figure 9e**), which favored the charge storage. Briefly, when the light was induced, the ReS_2 nanosheets absorbed the light and generated the electron-hole pairs. Then, the generated electron-hole pairs separated by the applied potential provided the extra charge carriers, thus allowing more electrolyte ions to accumulate at the electrode/electrolyte interface and contributing to the enhancement of capacitor behavior.[30]

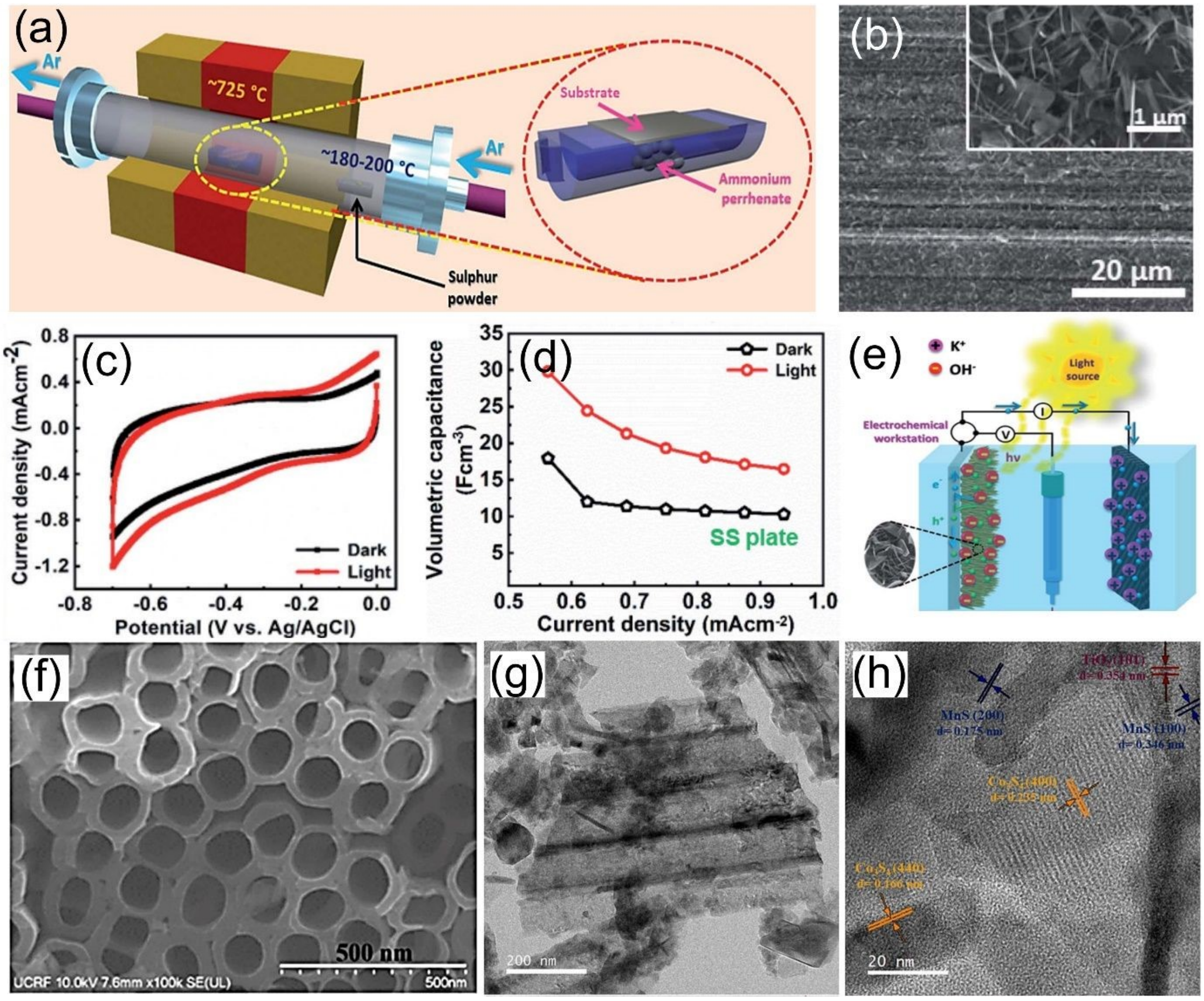

Figure 9. (a) Illustration of growth of ReS_2 *via* CVD method, (b) SEM images of ReS_2 grown on stainless steel. (c) CV curves of ReS_2 electrode at 100 $mV \cdot s^{-1}$ in dark and light conditions. (d) Rate capability of ReS_2 electrode in the dark and light conditions. (e) Illustration of the mechanism for light-induced energy storage in ReS_2.[30] Reproduced with permission.[30] Copyright 2021, Royal Society of Chemistry. (f) SEM image of the CoMnS decorated on TiO_2 nanotubes and corresponding (g) low-resolution and (h) high-resolution TEM images.[99] Reproduced with permission.[99] Copyright 2024, Elsevier.

Furthermore, bi-/ter-nary metal sulfides were also promising candidates as photo-electrodes for photo-assisted SCs due to their desirable optimal band gap, higher absorption coefficient, and higher capacitance compared with mono-metal sulfides. Binary CoMnS decorated on TiO_2

View Article Online
DOI: 10.1039/D61A00650G

nanotubes (**Figure 9f-9h**) were prepared as photoelectrodes for photo-assisted SCs.[99] Based on the testing results, the photo-assisted SCs can simultaneously harvest light and effectively store charge to provide enhanced capacitor behavior in terms of prolonged discharge time, capacity enhancement (70% increment), and good cycle life under light irradiation.[99] In addition, ternary Cu_2ZnSnS_4 synthesized by a simple and mild solvothermal reaction was employed as photo-electrode for the construction of photo-assisted SCs.[100] It was noted that with the light irradiation, the optimized Cu_2ZnSnS_4 electrode displayed a significant enhancement in the capacitor behaviour including a larger area enclosed by the CV curve, a higher specific capacitance, and a lower interfacial charge transfer resistance in comparison to the dark condition.

3.3.3 Metal oxides for photo-responsive SCs

Apart from conducting polymers and metal sulfides, metal oxides were widely employed to fabricate light-responsive smart SCs with enhanced energy storage performance. Metal oxides (e.g., TiO_2, ZnO, Fe_2O_3, V_2O_5) are well-known semiconductors that can absorb ultraviolet light and generate electron-hole pairs. In the photo-enhanced SCs, the internal electric field helped separate the photo-generated charges. This effectively increased the number of charge carriers available for the electrochemical reactions, resulting in the enhanced capacitor behavior compared to the metal oxide electrodes tested in the absence of light. Moreover, nanoengineering metal oxides into various forms, morphologies, and structures can also enhance the performance of as-prepared photo-responsive SCs by boosting the rate of photo-assisted charge transfer reactions, increasing the interaction between active material and electrolyte, and facilitating ion diffusion.

As one of the commonly used metal oxides, WO_3 with a narrow band gap can not only absorb visible light to generate electron-hole pairs but also react with some small cations to form the tungsten bronze, thus exhibiting a unique photochromic property. In this case, WO_3 was expected to be a promising candidate material for designing photo-responsive SCs. As a proof-of-concept, WO_3 synthesized by using a microwave-assisted hydrothermal method served as a photo-electrode for the construction of photo-responsive SCs (**Figure 10a**).[101] The electrochemical performance of WO_3-based SCs was improved under solar light, as evidenced by an increase of the area surrounded by the CV curve (**Figure 10b**) and a prolonged discharge time based on the charge/discharge curves (**Figure 10c**). According to the energy storage kinetic analysis, the photoexcited electrons not only facilitated the insertion of protons into

View Article Online
DOI: 10.1039/D5TA00650G

WO_3 during charging but also accelerated the discharging kinetics. The specific effect of light illumination on the capacitive behavior of the WO_3-based SCs can be explained as follows (**Figure 10d**). When the WO_3-based electrode was exposed to light and absorbed the light energy, electron-hole pairs were generated at the same time. During the charging process, the generated electrons were transferred to the electrode/electrolyte interface and subsequently caused the reduction of WO_3 by accompanying the insertion of protons. On the contrary, during the discharge process, the stored electrons are released, and the inserted protons are extracted back into the electrolyte, corresponding to a reversible proton-coupled electron storage process. Therefore, the kinetics of the charging/discharging process of the WO_3-based SCs can be sped up under the light illustration.[101]

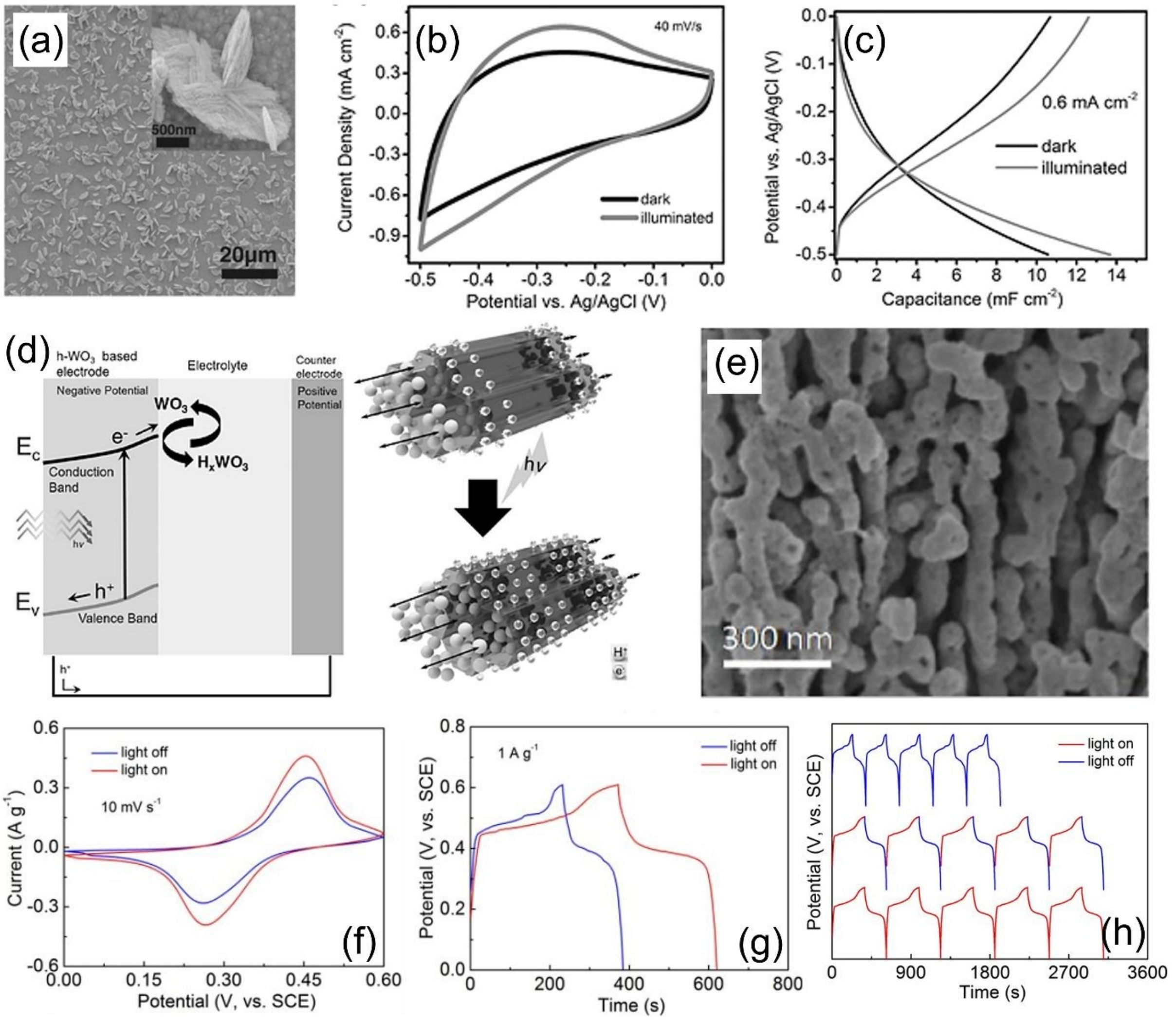

Figure 10. (a) SEM image of h-WO_3 film grown on fluorine-doped tin oxide (FTO). (b) CV curves and (c) charge/discharge curves of the obtained h-WO_3 film electrode in dark condition and under illumination with solar light, respectively. (d) Illustration of the increments of capacitance for h-WO_3 film electrode under illumination of solar light.[101] Reproduced with permission.[101] Copyright 2016, Wiley-VCH. (e) SEM image of 3D nanoporous Cu@Cu_2O

View Article Online
DOI: 10.1039/D6TA00650G

composite electrode. (f) CV curves and (g) charge/discharge curves of the 3D nanoporous $Cu@Cu_2O$ electrode under dark condition and light illumination. (h) Charge/discharge profiles of the 3D nanoporous $Cu@Cu_2O$ electrode under dark condition and light illumination.[102] Reproduced with permission.[102] Copyright 2019, Royal Society of Chemistry.

Moreover, the performance of metal oxides can be improved through various strategies such as preparing the composite, which can facilitate the electron-hole pair separation and allow for more efficient absorption of visible light. As a representative example, the Mn_3O_4/rGO composite exhibited an 82% increase in capacitance in light condition compared to that in dark condition.[49] The increment in capacitance was mainly due to the photoexcitation of electrons when an external light source was applied. In brief, when an external light source fell on the active region of the electrode, the electron-hole pairs were separated during the charge/discharge process, thus accelerating the photo excitation and enhancing the capacitance.[49] Furthermore, nanoengineering metal oxides with specific morphology and structures was also conducive to boost the performance of as-prepared photo-responsive SCs. In view of this, a photo-responsive SCs was constructed using a 3D nanoporous $Cu@Cu_2O$ array (**Figure 10e**) as the working electrode.[102] Electrochemical results showed that, with the aid of the solar light, the current densities of redox peaks in the CV curves increased (**Figure 10f**), and the voltage difference between the oxidation and reduction peaks decreased, indicating enhanced capacitance and improved reversibility. Also, noted that the device exhibited a lower charge voltage plateau, a higher discharge plateau, and a longer discharge time (**Figure 10g**), further demonstrating the improved reversibility and enhanced capacitance under the light illumination. Furthermore, the comparative experiment (**Figure 10h**) showed that light significantly affected the charging process. The mechanism underlying the performance improvement of the 3D nanoporous $Cu@Cu_2O$ electrode under solar light illumination was briefly described as follows. Under the light illumination, the semiconductor Cu_2O generated electron-hole pairs, in which the photo-generated holes oxidized Cu_2O to CuO, while the photo-generated electrons passed through the external circuit and produced H_2 by reduction reaction. The corresponding discharge process was the inverse procedure. Herein, the 3D nanoporous $Cu@Cu_2O$ electrode design provided a new solution for the construction of photo-responsive energy storage devices.[102]

View Article Online
DOI: 10.1039/D6TA00650G

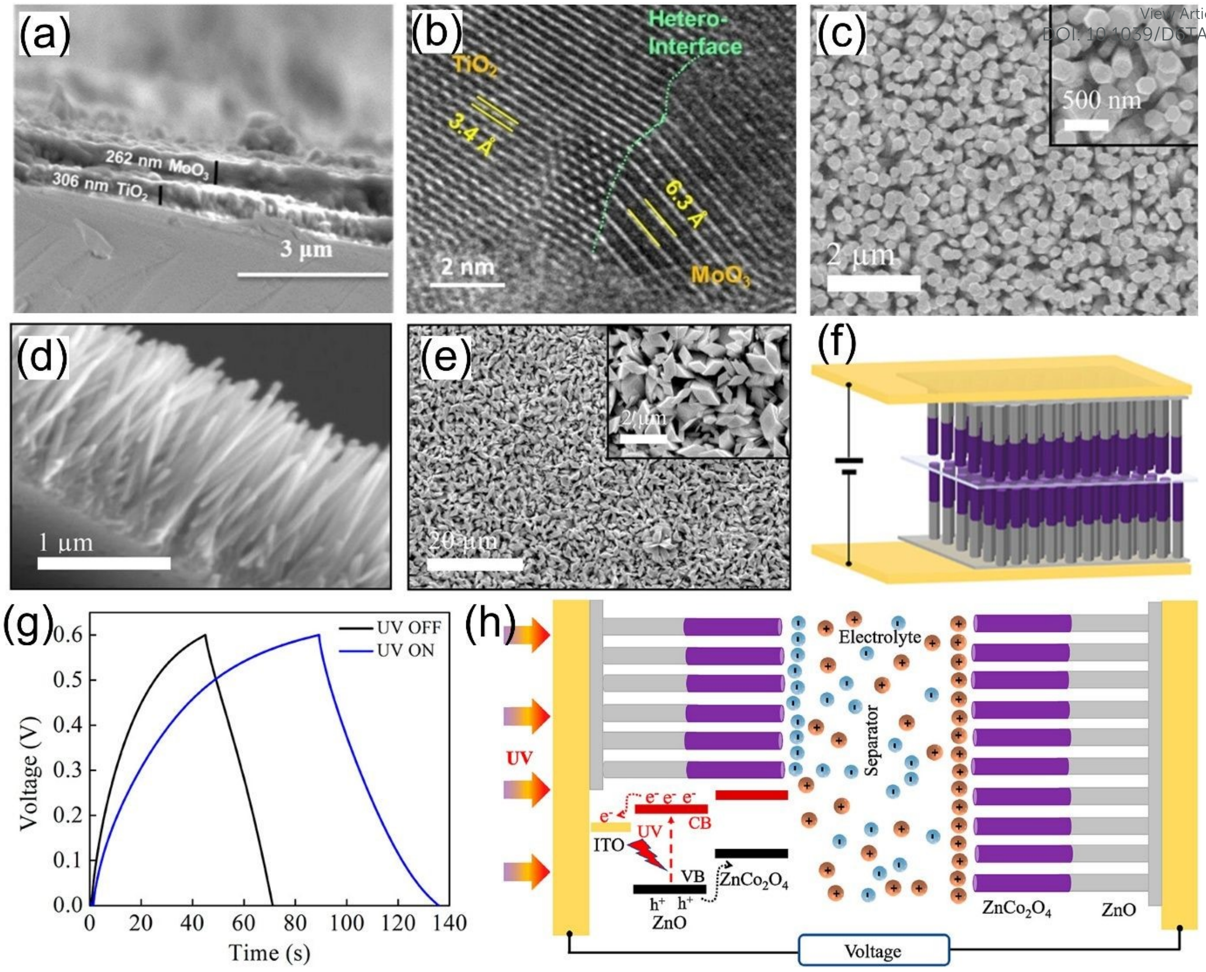

Figure 11. (a) Cross-sectional SEM image and (b) TEM image of CeO_2/MnO_2 heterojunction.[104] Reproduced with permission.[104] Copyright 2025, Wiley-VCH. (c) SEM image of as-grown ZnO nanoarrays. (d) Cross-sectional SEM image and (e) corresponding low and high magnification SEM images of the $ZnO/ZnCo_2O_4$ nanoarrays. (f) Illustration of the assembled SCs based on two $ZnO/ZnCo_2O_4$ nanoarrays. (g) Charge/discharge curves of the obtained SCs with and without UV light. (h) Illustration of the mechanism of the photo-responsive SCs based on $ZnO/ZnCo_2O_4$ nanoarrays under UV light.[108] Reproduced with permission.[108] Copyright 2019, American Chemical Society.

Although photo-active electrode materials can generate the electron-hole pairs under light illumination, the carrier separation was very important for the generated carriers to reach the electrode where they were collected. In this case, minimizing the recombination rate can achieve better performance of the device. As reported, the interface design was a better option to reduce the recombination rate of the photo-active electrode. In this way, the design of heterojunction photoresponsive electrodes, especially the type II heterojunction,[103] was able to offer significant performance enhancements over the single-material electrodes, primarily by improving the efficiency of charge separation and transport. First, a built-in electric field

View Article Online
DOI: 10.1039/D6TA00650G

formed at the interface between two different materials acted as a driving force to separate the electron-hole pairs, thus significantly suppressing their recombination and ensuring more carriers to participate in the reactions. Second, the heterojunction electrodes can absorb light over a wider range of the electromagnetic spectrum, making more efficient utilization. Hence, a bi-layer TiO_2/MoO_3 heterojunction electrode was designed with a simple sol-gel and spin coating method (**Figure 11a, 11b**).[104] The typical CV curves of TiO_2/MoO_3 heterojunction electrode revealed faster redox reaction and larger energy storage capability under UV illumination. The enhanced kinetics under light illumination can be briefly described as follows. When the TiO_2/MoO_3 electrode absorbed the light, the electron-hole pairs were generated. Subsequently, the generated carriers were effectively separated under the internal driving force, of which the generated electrons transferred to the surface of the electrode while the holes moved towards the counter electrode and then got neutralized by the proton. Obviously, the light illumination had a significant impact on the diffusion-controlled process (proton insertion and charge carrier separation) rather than the surface (proton) adsorption process.[104] Similarly, a carbon fiber paper-supported CeO_2/MnO_2 heterojunction electrode was successfully synthesized by a two-step in-situ growth process.[105] Encouragingly, the obtained CeO_2/MnO_2 electrode not only displayed enhanced capacitor behaviors ($303\ F\cdot g^{-1}$ at $0.25\ A\cdot g^{-1}$) and good cycling stability but also maintained 56% of the light-enhanced capacitance even after half a day of light irradiation. The photo-induced capacitor enhancement was attributed to the well-designed CeO_2/MnO_2 heterojunction, which not only offered the additional photo-induced charge carriers under light irradiation, but also facilitated the charge carriers' separation, thus improving its photo-assisted charging capability.[105]

As reported, the unique 3D structure facilitated efficient electron-hole separation, thus allowing the charge carriers to be used for energy conversion.[106, 107] Importantly, the 3D structure provided interconnected charge transport channels, thus promoting the migration of carrier. Moreover, the high surface area increased the number of active sites and enhanced the light absorption. Given this, the design and preparation of 3D structural electrodes was able to boost the capacitive behavior of the device compared with that based on the other dimensional electrodes. As a representative example, $ZnO/ZnCo_2O_4$ nanoarrays (**Figure 11c-11e**) were prepared using the hydrothermal method to serve as the photo-active electrodes of SCs (**Figure 11f**).[108] Under the UV light exposure, the increased area enclosed by the deviated rectangular CV curve indicated the enhanced capacitor behavior and the existence of fast surface redox reactions on this electrode. Furthermore, the increased discharge time in the presence of UV

View Article Online
DOI: 10.1039/D6TA00650G

exposure further confirmed the enhancement of the capacity (**Figure 11g**). The working mechanism of the device under UV exposure was shown as follows (**Figure 11h**). Under the UV illumination, the photo-generated electrons transferred from ZnO to indium tin oxide (ITO) and passed through the external circuit, while the generated holes moved from ZnO to $ZnCo_2O_4$ due to the internal electric field in the heterojunctions. Subsequently, electrons at the negative electrode promoted the formation of an electrical double layer at the ZnO/$ZnCo_2O_4$ electrode/electrolyte interface, while the holes at the positive electrode participated in surface-related reactions and the formation of the electrical double layer. Therefore, it can be concluded that the exposure of ZnO/$ZnCo_2O_4$ under UV light can improve electron transport efficiency and enhance the charge storage capacity of the electrode.[108] Based on the above analysis, the strategies proposed in this section provided new insights into the design of high-performance photoresponsive smart SCs (**Table 4**), which were expected to be applied to next-generation energy storage devices. Meanwhile, the photo-induced capacitive enhancement opened new avenues for advancing photoresponsive supercapacitor technology by leveraging the synergistic effect of photoactivity and electrochemical performance.

Table 4. Electrochemical performance comparison of photo-responsive SCs.

Electrode material	Electrolyte	Potential window (V)	Capacitance ($F \cdot g^{-1}$)		Ref.
			Without light illumination	With light illumination	
Thieno [3,2-b] thiophene BODIPY	1 M KOH	-0.85-0.1	86 (1 A $\cdot g^{-1}$)	134 (1 A $\cdot g^{-1}$)	[14]
FBP_allyl_X electrode	1 M H_2SO_4	0-1.0	190.2 (1 A $\cdot g^{-1}$)	369.8 (1 A $\cdot g^{-1}$)	[97]
3D graphene/PEDOT:PSS electrode	PVA/H_3PO_4 electrolyte	0-0.8	534 $mF \cdot cm^{-3}$ (3.3 $mA \cdot cm^{-3}$)	699.3 $mF \cdot cm^{-3}$ (3.3 $mA \cdot cm^{-3}$)	[98]
Vertically aligned ReS_2 nanosheets	1 M KOH	-0.7-0	1.12 $mF \cdot cm^{-3}$ (0.375 $mA \cdot cm^{-2}$)	21.1 $F \cdot cm^{-3}$ (0.375 $mA \cdot cm^{-2}$)	[30]
CoMnS/TiO_2 nanotubes	3M KOH	0-0.55	42.2 $mF \cdot cm^{-3}$ (0.7 $mA \cdot cm^{-2}$)	71.7 $F \cdot cm^{-3}$ (0.7 $mA \cdot cm^{-2}$)	[99]
Cu_2ZnSnS_4	1 M KCl	-0.1-0.5	41.7 $F \cdot g^{-1}$ (5 $mV \cdot s^{-1}$)	33.8 $F \cdot g^{-1}$ (5 $mV \cdot s^{-1}$)	[100]
WO_3 nanosheets	0.5 M H_2SO_4	-0.5-0	15.3 $mF \cdot cm^{-3}$ (0.15 $mA \cdot cm^{-2}$)	17.8 $F \cdot cm^{-3}$ (0.15 $mA \cdot cm^{-2}$)	[101]
Mn_3O_4/rGO composite	0.5 M KOH	-0.4-0.6	21.9 (0.5 A $\cdot g^{-1}$)	13.8 (0.5 A $\cdot g^{-1}$)	[49]
3D nanoporous Cu@Cu_2O array	2 M KOH	0-0.6	567 (1 A $\cdot g^{-1}$)	782 (1 A $\cdot g^{-1}$)	[102]
TiO_2/MoO_3 heterojunction	0.5 M H_2SO_4	-0.5-0	38.6 $mF \cdot cm^{-3}$ (0.1 $mA \cdot cm^{-2}$)	63.2 $F \cdot cm^{-3}$ (0.1 $mA \cdot cm^{-2}$)	[104]
CeO_2/MnO_2 heterojunction	1 M Na_2SO_4	0-0.8	187 $F \cdot g^{-1}$ (5 $mV \cdot s^{-1}$)	229 $F \cdot g^{-1}$ (5 $mV \cdot s^{-1}$)	[105]
ZnO/$ZnCo_2O_4$ nanoarrays	PVA-KOH electrolyte	0-0.6	86 $\mu F \cdot cm^{-2}$ (1.2 $\mu A \cdot cm^{-2}$)	150 $\mu F \cdot cm^{-2}$ (1.2 $\mu A \cdot cm^{-2}$)	[108]

View Article Online
DOI: 10.1039/D6TA00650G

3.4. Potential-responsive SCs

Since electrochromic devices underwent reversible color change under the influence of potential, they provided a good opportunity to design the potential-responsive smart SCs, which can be used both as a color-indicator and an energy storage device. As reported, the performance of the potential-responsive smart SCs relied on the electron transfer and the electrolyte ion transfer of the electrochromic materials during the electrochemical redox reactions. Therefore, the design of nanostructured electrochromic materials with specific structure/morphology, crystal phase design, high specific area, and high electronic conductivity were beneficial to achieving high-performance smart potential-responsive SCs.

3.4.1 Metal oxide-based materials for potential-responsive SCs

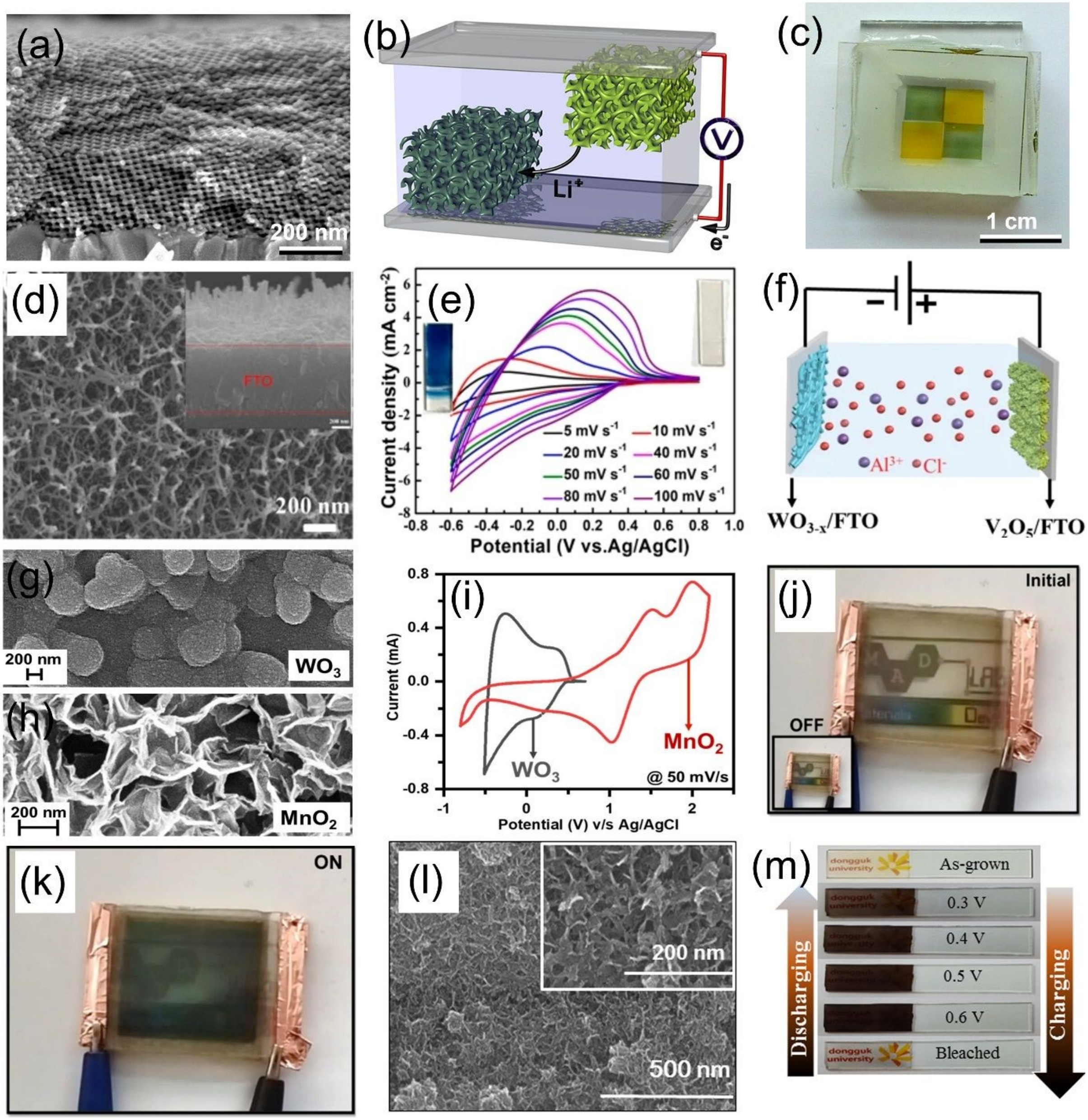

View Article Online
DOI: 10.1039/D6TA00650G

Figure 12. (a) Cross-sectional SEM image of mesoporous V_2O_5 double-gyroid film. (b) Illustration of the SCs based on V_2O_5 double-gyroid film electrodes. (c) Photograph of a transparent electrochromic SCs.[112] Reproduced with permission.[112] Copyright 2012, American Chemical Society. (d) SEM image of WO_{3-x} NWNs/FTO electrode and its corresponding (e) CV curves under different scan rates. (f) Illustration of the assembly of an electrochromic SCs device using WO_{3-x} NWNs/FTO anode and V_2O_5 nanoflowers/FTO cathode.[113] Reproduced with permission.[113] Copyright 2021, Springer Nature. SEM images of (g) WO_3 electrode and (h) MnO_2 electrode. (i) CV curves of WO_3 electrode and MnO_2 electrode at 50 $mV \cdot s^{-1}$. Photographs of the device based on WO_3 electrode and MnO_2 electrode in (j) initial state and (k) ON state.[114] Reproduced with permission.[114] Copyright 2025, American Chemical Society. (l) SEM images of the $NiMoO_4$ film. (m) Photograph of the $NiMoO_4$ electrode bleached at different voltage potentials.[115] Reproduced with permission.[115] Copyright 2018, Elsevier.

As mentioned before, the electrode materials for potential responsive SCs should possess both electrochromic and energy storage properties. Among these developed electrochromic materials, transition metal oxides (e.g., V_2O_5, WO_3, MnO_2, NiO, TiO_2),[109-111] which caused color change through bandgap change by electrochemical oxidation/reduction reaction, were widely used. Noted that nanomaterials with large surface area and suitable porosity can improve the electrochromic efficiency by reducing resistance during the charge and mass transport processes. As such, a free-standing V_2O_5 network with the double-gyroid morphology was obtained by electrodeposition into a hollow block copolymer template (**Figure 12a**).[112] The transparent electrochromic Li-ion SCs (**Figure 12b**), which were assembled by V_2O_5 electrodes with the gyroid-structure grown on FTO substrate, displayed the yellow color in the oxidized state while exhibiting a green/gray color in the reduced state (**Figure 12c**). Moreover, the obtained Li-ion SCs exhibited a high specific capacitance (155 $F \cdot g^{-1}$ at 10 $A \cdot g^{-1}$) and a high energy density of 52 $Wh \cdot kg^{-1}$. Its excellent electrochemical performance was attributed to the V_2O_5 electrode with interconnected porosity, good electronic transport, and large surface area, which reduced the Li^+ ion transport distance and enabled the fast lithium-ion insertion/extraction. Owing to the unique color changing during the charging/discharging process, the V_2O_5-based electrochromic SCs are a promising candidate for the design of smart voltage-responsive SCs.[112]

Apart from symmetric electrochromic SCs, it was also a feasible option to construct the electrochromic SCs using suitable asymmetric electrode materials. A full device was assembled by coupling V_2O_5 nanoflowers/FTO cathode with WO_{3-x} NWNs/FTO anode (**Figure 12d, 12e**).[113] The device (**Figure 12f**) delivered a specific areal capacitance of 18.5 $mF \cdot cm^{-2}$ (1 $mA \cdot cm^{-2}$) and kept a specific areal capacitance of 5.44 $mF \cdot cm^{-2}$ (4 $mA \cdot cm^{-2}$), which overperformed some of the reported smart electrochromic SCs. It was interesting to note

View Article Online
DOI: 10.1039/D6TA00650G

that the color of the device gradually turned to dark blue during charging, while it gradually became transparent during discharging, which was attributed to the insertion and extraction of Al^{3+} ions. The results presented here proved the possibility of the construction of voltage-response smart SCs with dual functions, which not only served as an energy storage device but also possessed the electrochromic properties.[113]

As another representative example, a new smart electrochromic SCs was constructed by using WO_3 negative electrode (**Figure 12g**) and MnO_2 positive electrode (**Figure 12h**).[114] The obtained device exhibited a color change from pale yellow to dark blue during the charging/discharging process (**Figure 12i**), which was due to the combined effect of the color change of the WO_3 negative electrode and the MnO_2 positive electrode (**Figure 12j, 12k**). For the WO_3 negative electrode, the insertion of Li^+ ions caused the reduction of W^{6+} to W^{5+} during the charging process, leading to the color change from transparent to blue, while it returned to its transparent state in the discharging process. Meanwhile, the color of MnO_2 electrode changed from pale yellow to dark brown during charging, corresponding to the oxidation of Mn^{3+} to Mn^{4+}, while during discharging, Mn^{4+} was electrochemically reduced to Mn^{3+}, leading to the pale-yellow color of the MnO_2 film due to the detachment of Li^+ ions. Excitingly, the smart electrochromic SCs also showed a high specific capacitance ($22.6\ mF\cdot cm^{-2}$) and excellent cycle stability. The superior electrochromic properties and the remarkable capacitor behavior suggested its huge potential for use as smart electrochromic SCs.[114]

In addition, the bi-metal oxides were also explored to design the voltage-responsive smart electrodes due to the synergistic effects between two different metal elements, thereby leading to enhanced performance in several key areas, such as more efficient charge transport during the coloring and bleaching processes, a wider potential range for redox reactions, and ultrahigh optical modulation across a broader range of the spectrum. As a proof-of-concept, a smart electrochromic SCs was built based on $NiMoO_4$ thin film electrode (**Figure 12l**),[115] which was prepared by a simple successive ionic layer adsorption and reaction technique. The nanoflake $NiMoO_4$ film electrode was dark brown in the charge state and became transparent in the discharged state (**Figure 12m**). Encouragingly, the nanoflake $NiMoO_4$ film electrode exhibited a high specific capacitance up to $1853\ F\cdot g^{-1}$ at $1\ A\cdot g^{-1}$ and a stable long-cycle performance. The remarkable electrochemical performance and fast and reversible color modulation enabled the design the voltage-responsive smart SCs.[115]

View Article Online
DOI: 10.1039/D6TA00650G

3.4.2 Conducting polymer-based materials for potential-responsive SCs

Although inorganic electrochromic materials have shown potential application in electrochromic SCs, they still suffer from some drawbacks, such as limited color changes and slow switching speeds, thus limiting their large-scale application. Fortunately, organic electrochromic materials, such as organic molecules, polymers, and organic frameworks,[116-118] have attracted tremendous attention as alternative materials for the electrochromic SCs because of their rich color selection, fast response rate, and relatively high capacity resulting from multiple redox sites. Representatively, PANI with excellent electrical conductivity was used as an active material for the design of voltage-responsive smart SCs. As an example, PANI film electrode was synthesized by a combination of galvanostatic and cyclic voltametric electrodeposition techniques (**Figure 13a**).[119] The film electrode exhibited multicolor properties with reversible color changes due to three main stable oxidation states of PANI: the fully oxidized pernigraniline form (purple), the 50% oxidized emeraldine form (green), and the fully reduced leucoemeraldine form (transparent yellow). As shown in CV curve (**Figure 13b**), the first oxidation peak (0.34 V) and reduction peak (0.10 V) were attributed to the doping and de-doping of anions, corresponding to the change between leucoemeraldine base and emeraldine salt, while the second oxidation peak (0.9V) and reduction peak (0.69 V) were associated with the conversion between emeraldine base and pernigraniline base. Furthermore, the color change between these two redox peaks was associated with the conversion of the emeraldine salt and emeraldine base arising from protonation/deprotonation processes (**Figure 13c**). Surprisingly, the PANI film electrode delivered a high specific capacitance (473.3 $\mathrm{F \cdot g^{-1}}$) at 30 $\mathrm{mV \cdot s^{-1}}$ and kept a relatively high capacitance (392.1 $\mathrm{F \cdot g^{-1}}$) at 150 $\mathrm{mV \cdot s^{-1}}$ (**Figure 13d**). Its superior electrochemical performance, combined with its multiple color states, made the PANI film electrode a promising candidate for the construction of potential-responsive SCs.[119]

Similarly, an electrochromic fiber-shaped SCs was constructed by wrapping aligned PANI/CNTs composite on an elastic fiber (**Figure 13e-13g**).[120] The obtained SCs exhibited rapid and reversible color changes, which were related to the different oxidation states of PANI. Taking the positive electrode as an example, the relationship between the color change and oxidation state was revealed. When the potential of the PANI/CNTs composite was charged to 1 V, the PANI was in a fully oxidized state, exhibiting a blue color; when the potential was discharged to 0.5 V, the PANI/CNTs composite was in the partially reduced state, showing a green color. Notably, when the electrode was further discharged to −0.5 V or −1 V, the PANI was in a highly reduced state, exhibiting a light yellow.[120] Additionally, new organic

View Article Online
DOI: 10.1039/D6TA00650G

conjugated polymers were attractive alternative candidate materials for constructing smart electrochromic SCs. With this in mind, a new conjugated polymer was synthesized *via* a simple electropolymerization method (**Figure 13h**).[121] Notably, the color of PETOME/ITO electrode changed during the electrochromic process: yellow in the anion-doped state (−0.3 V), green in the neutral state (0 V), and finally blue in the cation-doped state (1.0 V) (**Figure 13i**), which indicated its multicolor electrochromic behavior due to the integration of EDOT and TPA dual-redox centers.[121] The almost symmetric triangle shape of the charge/discharge curves (**Figure 13j**) demonstrated fast electrochemical reaction kinetics and excellent capacitor behavior, which was attributed to the twisted arrangement of the TPA structure, thereby accelerating ions diffusion and reaction kinetics. Encouragingly, coupled with a V_2O_5 nanowire cathode, an asymmetric electrochromic SC was built, which delivered a large potential window (2V), a high energy density (20.2 μWh·cm^{-2}), and a high optical contrast (71.4%). Therefore, it was reasonable to conclude that the rich color change and the remarkable electrochemical performance made the conjugated polymer-based electrode a promising candidate for the design of smart SCs combining energy storage and electrochromic.

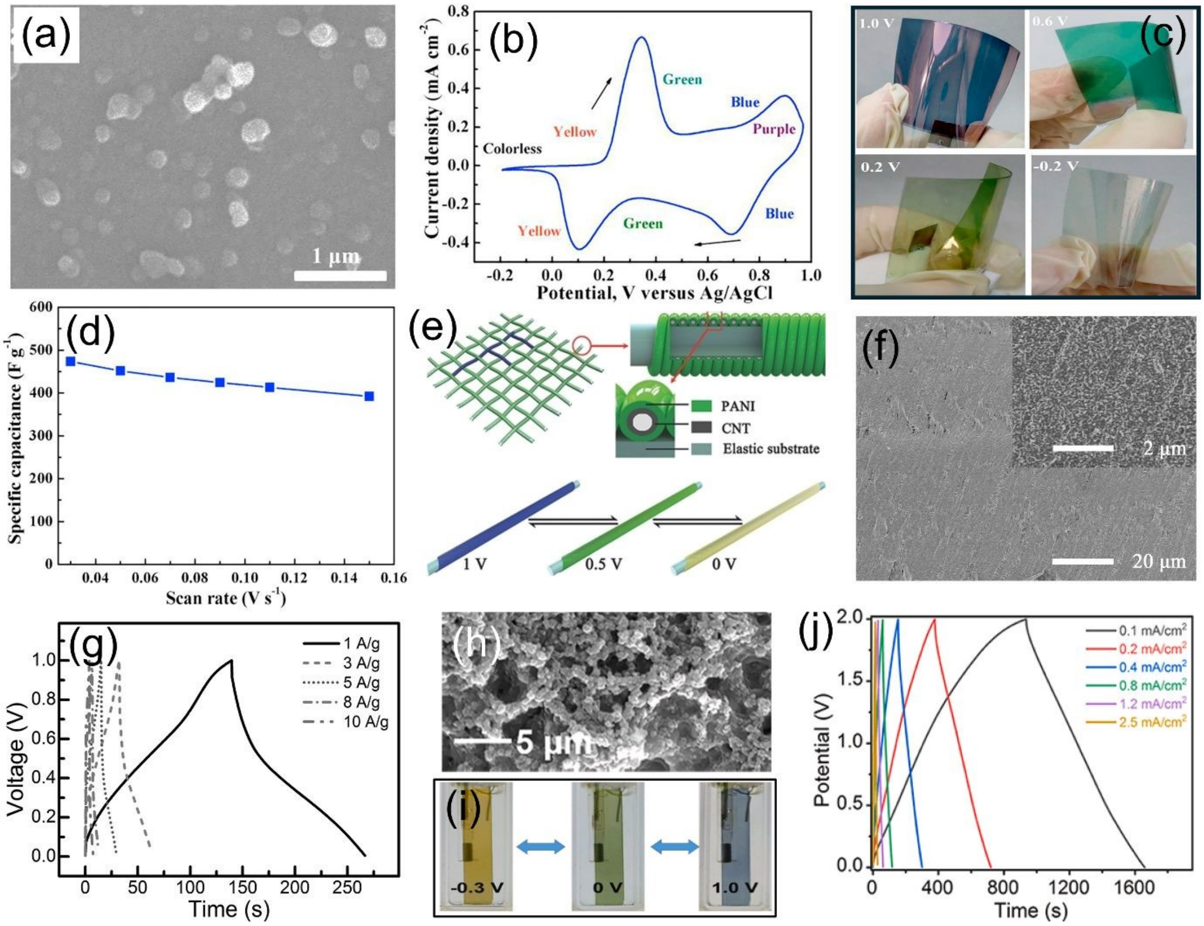

Figure 13. (a) SEM images of the as-prepared PANI film. (b) CV curve of the as-prepared PANI film electrode. (c) Photography of the PANI film in color under different potential states. (d) Rate capability of the PANI film electrode.[119] Reproduced with permission.[119] Copyright 2018, Elsevier. (e) Illustration of the structure of the electrochromic SCs based on CNT/PANI fiber. (f) SEM images and (g) charge/discharge curves of the optimized CNT/PANI composite electrode.[120] Reproduced with permission.[120] Copyright 2014, Wiley-VCH. (h) SEM image of the PETOME/ITO electrode and its corresponding (i) photography under different potential state and (j) charge/discharge curves.[121] Reproduced with permission.[121] Copyright 2023, Elsevier.

3.4.3 Composite-based materials for potential-responsive SCs

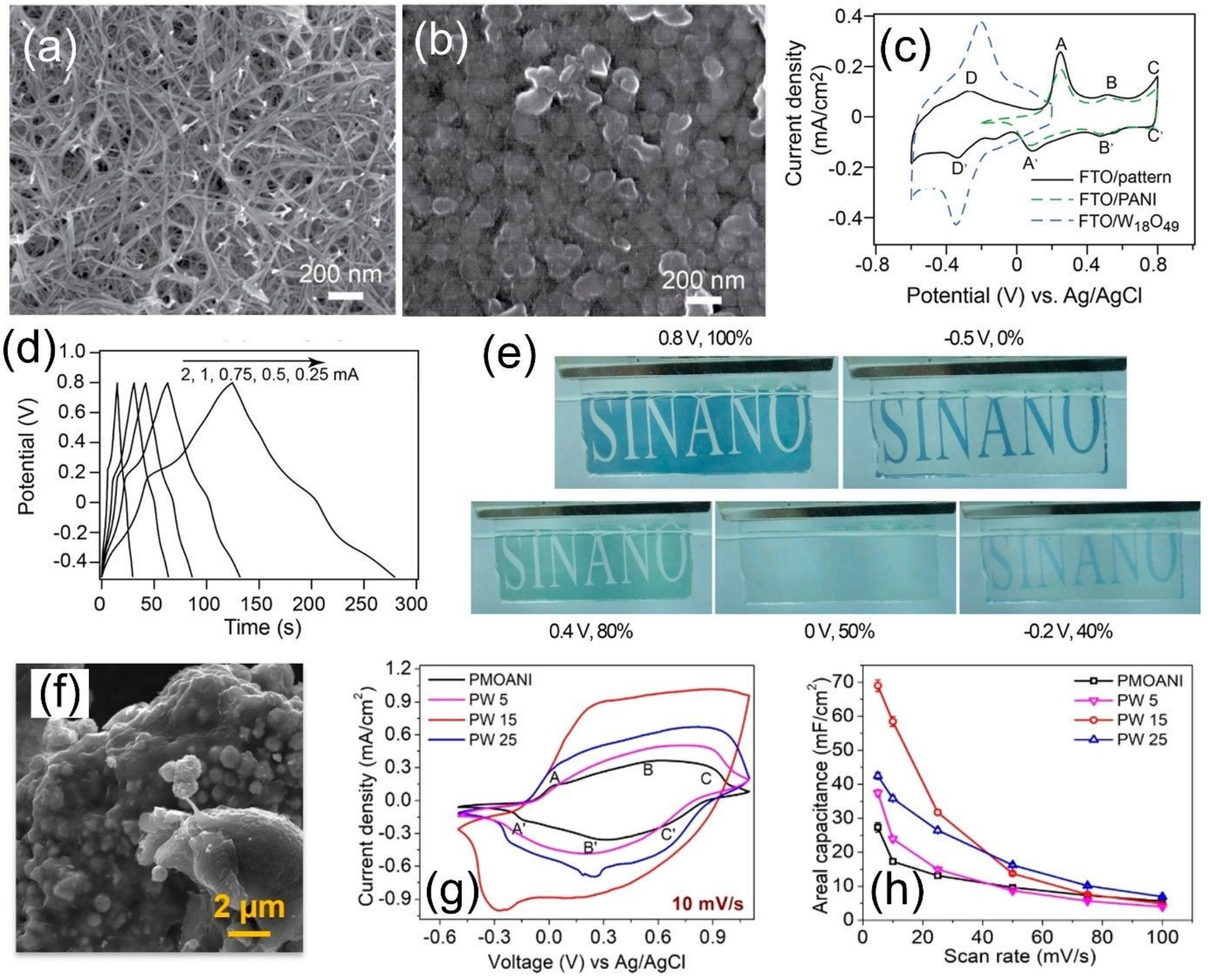

Figure 14. SEM images of (a) PANI film and (b) PANI/$W_{18}O_{49}$ composite. (c) CV curves of FTO, PANI, $W_{18}O_{49}$ electrodes, respectively. (d) Charge/discharge curves of the smart SCs based on PANI/$W_{18}O_{49}$ composite. (e) Photography of the SCs electrode at several typical states.[122] Reproduced with permission.[122] Copyright 2014, American Chemical Society. (f) SEM image of the PMOANI-WO_3 nanocomposite. (g) CV comparisons of different PMOANI-WO_3 nanocomposites at 10 mV·s^{-1}. (h) Areal capacitance of the SCs at different scan rates.[123] Reproduced with permission.[123] Copyright 2023, American Chemical Society.

View Article Online
DOI: 10.1039/D5TA00650G

As reported, transition metal oxides possessed some shortcomings, such as long response time and limited color variations. In contrast, conducting polymers have caused increasing attention due to their rich color variations and relative high capacitance. Nevertheless, conducting polymers suffered from irreversible mechanical degradation and capacity decay because of the repeating doping/de-doping of ions during the redox process. The design of a composite in which a transition metal oxide and a conductive polymer were combined was another effective strategy to build the voltage-responsive smart SCs having enhanced properties by the synergistic effects.[61] For instance, a smart electrochromic electrode based on the composite of $W_{18}O_{49}$ and PANI was well designed and constructed (**Figure 14a, 14b**).[122] It can be observed that the $W_{18}O_{49}$ displayed the electrochromic behavior in the potential range from −0.5 to 0 V, while the PANI showed the multicolor behavior in the potential range from 0 to 0.8 V (**Figure 14c**). Interestingly, the composite electrode prepared with $W_{18}O_{49}$ and PANI delivered a wide potential range (**Figure 14d**), possessed a high specific capacitance and displayed various colors (**Figure 14e**). By integrating the $W_{18}O_{49}$ and PANI into one electrode, the obtained composite electrode not only exhibited excellent capacitive behaviour but also enabled the electrode with new functionality in coloring, thus beneficial for the design and construction of high-performance smart electrochromic SCs.[122] Similarly, a facile and low-cost chemical polymerization strategy was employed to prepare a stable and active electrochromic composite material consisting of poly(o-methoxyaniline) (PMOANI) and WO_3 nanoflowers (**Figure 14f**).[123] The optimized polymer composite not only exhibited the pseudocapacitive property (**Figure 14g**) with a large areal capacitance (83 $mF\cdot cm^{-2}$) (**Figure 14h**) and good cycle life but also displayed color changing characteristic. Amazingly, an asymmetric SCs device built by this polymer composite exhibited an areal capacitance of 730 $\mu F\cdot cm^{-2}$ and can switch the color between blue and transparent green. The obtained SCs were expected to be an energy storage device with an additional color indication function, thus making it possible to design potential-based smart SCs.[123]

Subsequently, a silver grid/PEDOT:PSS/WO_3 composite film was fabricated through a unique design.[124] Notably, this film exhibited a noticeable electrochromic property and a high optical modulation (81.9%), making it highly suitable for electrochromic devices. Using the silver grid/PEDOT:PSS/WO_3 composite as an electrode in an electrochromic SCs, it was observed to exhibit a dark blue color during discharging and a transparent color during charging. The charge and discharge processes were related to the insertion and extraction of H^+ in WO_3 film. Specifically, the insertion of H^+ led to the reduction of the W^{6+} ions, thus causing the

WO_3 film to appear dark, which corresponds to the decrease in transmittance. During the discharging, the extraction of H^+ from the WO_3 film meant to be oxidized back to a higher valence state, which resulted in the transparent color, accompanied by an increased transmittance. The silver grid/PEDOT:PSS/WO_3 hybrid film delivered a specific capacitance of 221.1 $F\cdot g^{-1}$ at 1 $A\cdot g^{-1}$, which was larger than those of previously reported WO_3 electrodes. The unique structure and configuration endowed the silver grid/PEDOT:PSS/WO_3 hybrid film with high optical modulation and remarkable capacitor behavior, thus making it a promising application in the construction of voltage-responsive smart SCs. According to the above demonstration, the construction of nanostructured electrochromic materials with the outstanding electron transfer and electrolyte ion transfer capability, unique structure/morphology, and high specific area were beneficial to achieving high-performance smart potential-responsive SCs with multi-functions (**Table 5**).

Table 5. Electrochemical performance comparison of potential-responsive SCs.

Electrode material	**Electrolyte**	**Potential window (V)**	**Capacitance (F·g^{-1})**	**Color changing**	**Ref.**
V_2O_5	1 M $LiClO_4$/propylene carbonate solution	2-4	155 (≥10 A·g^{-1})	Green/gray/yellow	[112]
V_2O_5 NFs/FTO	1 M $AlCl_3$	-0.2-0.8	5.64 mF·cm^{-2} (5 mV·s^{-1})	Light green/transparent	[113]
WO_{3-x} NWNs/FTO	1 M $AlCl_3$	-0.6-0.8	57.6 mF·cm^{-2} (5 mV·s^{-1})	Dark blue/transparent	[113]
WO_3 (anode)	5% PEO + 1 M $LiClO_4$	−0.5-0.7	22.8 mF·cm^{-3} (0.1 mA·cm^{-2})	Transparent/blue	[114]
MnO_2 (cathode)	5% PEO + 1 M $LiClO_4$	−0.8-2.2	8.2 mF·cm^{-3} (0.1 mA·cm^{-2})	Pale yellow/dark brown	[114]
$NiMoO_4$ thin film	2 M KOH	-0.5-0.7	1853 (1A·g^{-1})	Transparent/dark brown	[115]
PANI film	0.5 M H_2SO_4	-0.2-1.0	473.3 (30 mV·s^{-1})	Transparent/yellow/green/blue/purple	[119]
PANI/CNTs composite	PVA/H_3PO_4 gel electrolyte	-1.0-1.0	255.5 (1 A·g^{-1})	Blue/green/light yellow	[120]
PETOME/ITO	0.1 M $LiClO_4$	−0.3-1.0	39 mF·cm^{-2} (0.1 mA·cm^{-2})	Yellow/green/blue	[121]
$W_{18}O_{49}$/PANI composite	1 M H_2SO_4	−0.5-0.8	24.6 mF·cm^{-2}	Transparent/blue	[122]
PMOANI/WO_3 nanoflowers	1 M $LiClO_4$–PC electrolyte	-1.0-1.0	16.3 mF·cm^{-2} (5 mV·s^{-1})	Blue/colorless	[123]
Silver grid/PEDOT:PSS/WO_3 composite	0.5 M H_2SO_4	-0.7-0.1	221.1 (1 A·g^{-1})	Blue/transparent	[124]

View Article Online
DOI: 10.1039/D6TA00650G

4. Future directions and conclusions

Currently, the smart stimuli-responsive SCs have attracted increasing attention due to their unique characteristics and multiple functions. Stimuli-responsive SCs are a new generation of energy storage devices whose electrochemical properties can be reversibly and intentionally modulated by applying external triggers like temperature, magnetic field, light, and voltage. These developments could create the next generation of energy storage technology that is not passive but capable of actively interacting with external stimuli, which is crucial for the wearable/portable devices.

The mechanism of smart SCs is to incorporate stimuli-responsive materials (e.g., metal oxides, smart polymers, photochromic molecules) into their electrode or electrolytes to induce reversible changes in their structure or properties, thereby adjusting or altering their capacitor behavior. Although the research of the primary types of external stimuli (e.g., temperature, magnetic field, light, voltage) and corresponding stimuli-responsive SCs has made significant progress, there are still a huge room left to further improve the performance of SCs: (a) For thermally responsive supercapacitors, the interfacial contact and electrochemical stability of thermally responsive polymer electrolytes is poor.[125, 126] Furthermore, the relatively low ionic conductivity affects the rate performance of the SCs. Moreover, further improvements in the switching response rate are needed to shorten the recovery time. Additionally, modifying the electrodes and separator with thermally responsive polymers results in energy density loss due to the weight of additional components; (b) For magnetically responsive SCs, although most research focused on understanding the effects of magnetic fields on the supercapacitive performance of materials, the origin of magnetic field-dependent supercapacitive properties remains controversial due to the involvement of many interfaces/components. In this context, a thorough investigation of the effects of magnetic fields on all properties of the electrodes and electrolytes is necessary; (c) For photoresponsive SCs, current research mainly focuses on exploring novel electrode materials, while interface design is often overlooked. This is because the performance of photoresponsive electrodes is highly dependent on their morphology, microstructure, and electrode/electrolyte interface. In addition, relatively low areal capacitance, low energy conversion efficiency and the complexity of integrated device design are also major challenges hindering their widespread application;[127] (d) Regarding the voltage-responsive SCs, achieving high performance in both electrochromism (color change) and supercapacitance (charge storage) is a challenging task. Typically, improving one property (e.g., coloring efficiency) compromises the other (e.g., specific capacitance). Furthermore, developing

View Article Online
DOI: 10.1039/D6TA00650G

electrolytes with a wide operating voltage window, high ionic conductivity, and excellent temperature stability remains a challenge.

Future research in stimuli-responsive SCs is focused on enhancing performance, durability, and multifunctionality for integration into next-generation smart electronics. Some key research directions are shown below: (i) A core direction is the development of novel stimuli-responsive materials (e.g., polymers with dynamic covalent bonding, specific hydrogels, novel hybrid materials) with tailored properties (e.g., conductivity, porosity, and response times) to push beyond traditional materials; (ii) In addition to the external stimuli mentioned in this review, exploring new stimuli (e..g, mechanical stress, pH) aims to leverage these external factors to overcome the limitations of SCs like low energy density, thus enhancing performance and enabling multifunctional energy storage devices; (iii) Future efforts are directed toward understanding the mechanism of the effect of these external stimuli on the resulting SCs, which is critical for the design of high-performance smart SCs. Therefore, more comprehensive studies are needed to reveal the crucial role of each external stimulus in dynamically controlling and optimizing the electrochemical processes, pushing beyond the performance limits of conventional SCs for specialized applications; (iv) This field is still quite new, and there is an urgent need to establish standardized testing procedures and performance benchmarks to ensure comparability between different research products. Moreover, leveraging the latest advances in design guided by theory, simulation, and machine learning will accelerate structural optimization and deepen the understanding of underlying mechanisms. Encapsulation and device-level integration represent another critical yet often overlooked challenge for the practical deployment of stimuli-responsive SCs. Unlike conventional SCs, these systems rely on dynamic interactions between active materials and external stimuli, which makes them particularly sensitive to environmental factors such as moisture, oxygen, mechanical deformation, and temperature fluctuations. Effective encapsulation must therefore strike a delicate balance between environmental protection and stimuli accessibility. For example, photoresponsive devices require optically transparent yet impermeable barriers, while thermally or mechanically responsive systems demand flexible and thermally conductive packaging materials that do not hinder their response behavior.[128] In addition, maintaining the long-term stability of electrolyte systems (e.g., hydrogels or polymer-based electrolytes) under encapsulated conditions remains a major challenge due to potential dehydration, leakage, or chemical degradation.[129,130] The integration of encapsulation layers can also introduce additional interfacial resistance and increase device weight, thereby compromising electrochemical performance.[131] Consequently, the development of advanced encapsulation strategies, such as multifunctional barrier materials, self-healing coatings, and flexible thin-film packaging, will be essential to ensure durability, reliability, and real-world applicability of smart stimuli-responsive SCs.[132]

In summary, this paper briefly reviews the latest research progress in the design of stimulus-responsive SCs, focusing primarily on the synthesis of stimulus-responsive electrodes and their response characteristics/functions. Furthermore, it discusses the role of various external forces/stimuli in enhancing capacitance performance, particularly their interactions with the components of SCs. Finally, this paper also outlines the challenges and future research directions in this field. In a word, this paper not only provides a reference for the design and construction of smart responsive SCs but also offers valuable information for other researchers in this field.

Conflicts of interest

There are no conflicts of interest to declare.

Acknowledgements

The authors would like to acknowledge the funding support from Nanyang Technological University Startup Grant, Singapore Ministry of Education Academic Research Fund Tier1 Grant (RS30/23), University of Waterloo and the Natural Science and Engineering Research Council of Canada.

References

1. J. He, L. Cao, J. Cui, G. Fu, R. Jiang, X. Xu and C. Guan, *Adv. Mater.*, 2024, **36**, 2306090.
2. M. Yu, Y. Peng, X. Wang and F. Ran, *Adv. Funct. Mater.*, 2023, **33**, 2301877.
3. P. Zhang, F. Zhu, F. Wang, J. Wang, R. Dong, X. Zhuang, O. G. Schmidt and X. Feng, *Adv. Mater.*, 2017, **29**, 1604491.
4. U. Jeong and Y. Yin, *Adv. Funct. Mater.*, 2020, **30**, 1907059.
5. H. Parsimehr and A. Ehsani, *Chem. Rec.*, 2022, **22**, e202200075.
6. P. Pandey, P. Ray, A. Sharma and M. Qureshi, *Appl. Phys. Lett.*, 2024, **124**, 140503.
7. J. Zhuang, M. R. Gordon, J. Ventura, L. Li and S. Thayumanavan, *Chem. Soc. Rev.*, 2013, **42**, 7421–7435.
8. C. Li, K. Wang, J. Li and Q. Zhang, *ACS Mater. Lett.*, 2020, **2**, 779–797.
9. Y. Zhou, H. Qi, J. Yang, Z. Bo, F. Huang, M. S. Islam, X. Lu, L. Dai, R. Amal, C. H. Wang and Z. Han, *Energy Environ. Sci.*, 2021, **14**, 1854–1896.
10. R. Wang, M. Yao and Z. Niu, *InfoMat*, 2020, **2**, 113–125.

11. J. C. Kelly, M. Pepin, D. L. Huber, B. C. Bunker and M. E. Roberts, *Adv. Mater.*, 2012, **24**, 886–889.
12. J. C. Kelly, R. Gupta and M. E. Roberts, *J. Mater. Chem. A*, 2015, **3**, 4026–4034.
13. V. Sharma, S. Biswas and A. Chandra, *Adv. Energy Mater.*, 2018, **8**, 1800573.
14. M. Özdemir, S. Uluçay, E. Sevimli, S. Altınışık, B. Köksoy, B. Yalçın and S. Koyuncu, *ACS Appl. Energy Mater.*, 2025, **8**, 17232–17245.
15. J. Muñoz, *Advanced Materials*, 2024, **36**, 2305546.
16. V. Kumar, S. Park, K. Parida, V. Bhavanasi and P. S. Lee, *Mater. Today Energy*, 2017, **4**, 41–57.
17. S. Guragain, B. P. Bastakoti, V. Malgras, K. Nakashima and Y. Yamauchi, *Chem. Eur. J.*, 2015, **21**, 13164–13174.
18. H. Zhang, W. Li, Q. Huang, G. Huang, Z. Chi and B. S. Li, *Dye. Pigment.*, 2021, **187**, 109128.
19. R. Zheng, Y. Wei, Z.-C. Zhang, Z.-Y. Wang, L.-L. Ma, Y. Wang, L. Huang and Y.-Q. Lu, *Responsive Mater.*, 2023, **1**, e20230017.
20. M. Deepa, R. Sharma, A. Basu and S. A. Agnihotry, *Electrochim. Acta*, 2005, **50**, 3545–3555.
21. W. Wu, S. Guo, J. Bian, X. He, H. Li and J. Li, *J. Energy Chem.*, 2024, **93**, 453–470.
22. H. Zhang, P. Xue, J. Liu and X. Xu, *ACS Appl. Energy Mater.*, 2021, **4**, 6116–6124.
23. V. H. Nguyen, R. Tabassian, S. Oh, S. Nam, M. Mahato, P. Thangasamy, A. Rajabi-Abhari, W.-J. Hwang, A. K. Taseer and I.-K. Oh, *Adv. Funct. Mater.*, 2020, **30**, 1909504.
24. D. Zhang, B. Ren, Y. Zhang, L. Xu, Q. Huang, Y. He, X. Li, J. Wu, J. Yang, Q. Chen, Y. Chang and J. Zheng, *J. Mater. Chem. B*, 2020, **8**, 3171–3191.
25. J. Wei, C. Ma, T. Zhang, Z. Shao and Y. Chen, *Chem. Eng. J.*, 2024, **490**, 151393.
26. H. Yang, Z. Liu, B. K. Chandran, J. Deng, J. Yu, D. Qi, W. Li, Y. Tang, C. Zhang and X. Chen, *Adv. Mater.*, 2015, **27**, 5593–5598.
27. Y. Dou, T. Pan, A. Zhou, S. Xu, X. Liu, J. Han, M. Wei, D. G. Evans and X. Duan, *Chem. Commun.*, 2013, **49**, 8462–8464.
28. Y. Shi, H. Ha, A. Al-Sudani, C. J. Ellison and G. Yu, *Adv. Mater.*, 2016, **28**, 7921–7928.
29. J. Zhu, M. Chen, H. Wei, N. Yerra, N. Haldolaarachchige, Z. Luo, D. P. Young, T. C. Ho, S. Wei and Z. Guo, *Nano Energy*, 2014, **6**, 180–192.
30. N. Arya, P. Avasthi and V. Balakrishnan, *Nanoscale Adv.*, 2021, **3**, 2089–2102.
31. Y.-J. Kim and Y. T. Matsunaga, *J. Mater. Chem. B*, 2017, **5**, 4307–4321.
32. D. Roy, W. L. A. Brooks and B. S. Sumerlin, *Chem. Soc. Rev.*, 2013, **42**, 7214–7243.
33. K. Ryu, G. Li, K. Zhang, J. Guan, Y. Long and Z. Dong, *Acc. Mater. Res.*, 2025, **6**, 379–392.
34. B. Wang, W. Liang, Z. Guo and W. Liu, *Chem. Soc. Rev.*, 2015, **44**, 336–361.
35. Y. Zhu, R. Batchelor, A. B. Lowe and P. J. Roth, *Macromol.*, 2016, **49**, 672–680.
36. Y. Hiruta, *Polym. J.*, 2022, **54**, 1419–1430.
37. T. Yu, P. Xue, S. Ma, Y. Gu, Y. Wang and X. Xu, *ChemistrySelect*, 2022, **7**, e202104499.
38. H. Jiang, R. K. Emmett and M. E. Roberts, *J. Appl. Electrochem.*, 2019, **49**, 271–280.
39. P. Zhang, J. Wang, W. Sheng, F. Wang, J. Zhang, F. Zhu, X. Zhuang, R. Jordan, O. G. Schmidt and X. Feng, *Energy Environ. Sci.*, 2018, **11**, 1717–1722.
40. Y. Yang, D. Yu, H. Wang and L. Guo, *Adv. Mater.*, 2017, **29**, 1703040.
41. J. Zhu, M. Yao, S. Huang, J. Tian and Z. Niu, *Angew. Chem. Int. Ed.*, 2020, **59**, 16480–16484.

42. Y. Shi, Q. Zhang, Y. Zhang, L. Jia and X. Xu, *ACS Appl. Mater. Interfaces*, 2018, **10**, 7171–7179.
43. S. Ma, Y. Shi, Y. Zhang, L. Zheng, Q. Zhang and X. Xu, *ACS Appl. Mater. Interfaces*, 2019, **11**, 29960–29969.
44. M. Li and Z. Chen, *J. Polym. Sci.*, 2021, **59**, 2230–2245.
45. Z. Chen, P.-C. Hsu, J. Lopez, Y. Li, J. W. F. To, N. Liu, C. Wang, Sean C. Andrews, J. Liu, Y. Cui and Z. Bao, *Nat. Energy*, 2016, **1**, 15009.
46. L. Zhang, Z. Zeng, D.-W. Wang, Y. Zuo, J. Chen and X. Yan, *Cell Rep. Phys. Sci.*, 2021, **2**, 100455.
47. S. Raj K A and C. S. Rout, *J. Mater. Chem. A*, 2023, **11**, 5495–5519.
48. K. M. Grant, J. W. Hemmert and H. S. White, *Electrochem. Commun.*, 1999, **1**, 319–323.
49. A. Joby, P. Kumbhakar and M. Balachandran, *Emerg. Mater.*, 2024, **7**, 2393–2406.
50. R. N. O'Brien and K. S. V. Santhanam, *J. Appl. Electrochem.*, 1997, **27**, 573–578.
51. G. Hinds, J. M. D. Coey and M. E. G. Lyons, *Electrochem. Commun.*, 2001, **3**, 215–218.
52. N. Leventis and X. Gao, *J. Am. Chem. Soc.*, 2002, **124**, 1079–1088.
53. S. Mohanta and T. Z. Fahidy, *J. Appl. Electrochem.*, 1978, **8**, 265–267.
54. C. M. Costa, K. J. Merazzo, R. Gonçalves, C. Amos and S. Lanceros-Méndez, *iScience*, 2021, **24**, 102691.
55. G. Hinds, F. E. Spada, J. M. D. Coey, T. R. Ní Mhíocháin and M. E. G. Lyons, *J. Phys. Chem. B*, 2001, **105**, 9487–9502.
56. P. Personnettaz, S. Landgraf, M. Nimtz, N. Weber and T. Weier, *Electrochem. Commun.*, 2019, **105**, 106496.
57. M. Waskaas and Y. I. Kharkats, *J. Phys. Chem. B*, 1999, **103**, 4876–4883.
58. S. C. Lau, H. N. Lim, T. B. S. A. Ravoof, M. H. Yaacob, D. M. Grant, R. C. I. MacKenzie, I. Harrison and N. M. Huang, *Electrochim. Acta*, 2017, **238**, 178–184.
59. R. Zhou, Y. Peng, X. Yang, Y. Yang, X. Li, Y. Gao, L. Wang and W. Lü, *J. Alloy. Compd.*, 2025, **1021**, 179587.
60. A. Bibi, M. Mustaqeem, M. A. Gondal, A. Majeed, P.-T. Chou, Y.-F. Chen, Z.-G. Gu, M. Waqas and A. Ali, *J. Energy Storage*, 2025, **123**, 116696.
61. M. Rakibuddin and H. Kim, *New J. Chem.*, 2017, **41**, 15327–15333.
62. A. Sood, A. D. Poletayev, D. A. Cogswell, P. M. Csernica, J. T. Mefford, D. Fraggedakis, M. F. Toney, A. M. Lindenberg, M. Z. Bazant and W. C. Chueh, *Nat. Rev. Mater.*, 2021, **6**, 847–867.
63. J. Li, Y. Zhuang, J. Chen, B. Li, L. Wang, S. Liu and Q. Zhao, *EnergyChem*, 2021, **3**, 100060.
64. W. Zhang, H. Li, E. Hopmann and A. Y. Elezzabi, *Nanophotonics*, 2021, **10**, 825–850.
65. M. Deepa, D. P. Singh, S. M. Shivaprasad and S. A. Agnihotry, *Curr. Appl. Phys.*, 2007, **7**, 220–229.
66. W. Kang, C. Yan, X. Wang, C. Y. Foo, A. W. Ming Tan, K. J. Zhi Chee and P. S. Lee, *J. Mater. Chem. C*, 2014, **2**, 4727–4732.
67. C. D. Wessells, R. A. Huggins and Y. Cui, *Nat. Commun.*, 2011, **2**, 550.
68. C. D. Wessells, S. V. Peddada, M. T. McDowell, R. A. Huggins and Y. Cui, *J. Electrochem. Soc.*, 2011, **159**, A98.
69. M. Qiu, F. Zhou, P. Sun, X. Chen, C. Zhao and W. Mai, *Nano Energy*, 2020, **78**, 105148.
70. X. Wang, L. Guo, S. Cao and W. Zhao, *Chem. Phys. Lett.*, 2020, **749**, 137434.
71. L. Striepe and T. Baumgartner, *Chem. Eur. J.*, 2017, **23**, 16924–16940.
72. S. Zhang, S. Chen, Y. Cao, F. Yang, H. Peng, B. Yan, H. Jiang, Y. Gu and M. Xiang, *J. Mater. Sci.: Mater. Electron.*, 2019, **30**, 13497–13508.

View Article Online
DOI: 10.1039/D6TA00650G

73. M. Tao, G. Liu, Y. Wang, J. Wang, W. Zhang and Z. Li, *ACS Appl. Mater. Interfaces*, 2024, **16**, 54316–54327.
74. M. Marzocchi, I. Gualandi, M. Calienni, I. Zironi, E. Scavetta, G. Castellani and B. Fraboni, *ACS Appl. Mater. Interfaces*, 2015, **7**, 17993–18003.
75. Z. Liu, H. I. Wang, A. Narita, Q. Chen, Z. Mics, D. Turchinovich, M. Kläui, M. Bonn and K. Müllen, *J. Am. Chem. Soc.*, 2017, **139**, 9443–9446.
76. A. Teixeira do Nascimento, P. R. Stoddart, T. Goris, M. Kael, R. Manasseh, K. Alt, J. Tashkandi, B. C. Kim and S. E. Moulton, *Adv. Mater.*, 2025, **37**, e07559.
77. S. Chen, Y. Li, Y. Feng and W. Feng, *Mater. Chem. Front.*, 2023, **7**, 1562–1590.
78. P. Yang, C. Feng, Y. Liu, T. Cheng, X. Yang, H. Liu, K. Liu and H. J. Fan, *Adv.Energy Mater.*, 2020, **10**, 2002898.
79. S. Tan, Z. Zhang, Y. Xue, J. Zhao, J. Ji, C. Wang and Y. Wu, *Ind. Eng. Chem. Res.*, 2023, **62**, 2741–2751.
80. S. Liu, S. Ma, Q. Zhang and X. Xu, *Ionics*, 2022, **28**, 5119–5128.
81. F. Mo, H. Li, Z. Pei, G. Liang, L. Ma, Q. Yang, D. Wang, Y. Huang and C. Zhi, *Sci. Bull.*, 2018, **63**, 1077–1086.
82. Q. Wang and L. Zhang, *ACS Nano*, 2021, **15**, 149–174.
83. M. Singh, A. Sahoo, K. L. Yadav and Y. Sharma, *ACS Appl. Mater. Interfaces*, 2020, **12**, 49530–49540.
84. P. Haldar, S. Biswas, V. Sharma and A. Chandra, *J. Electrochem. Soc.*, 2018, **165**, A3230.
85. A. González, E. Goikolea, J. A. Barrena and R. Mysyk, *Renew. Sustain. Energy Rev.*, 2016, **58**, 1189–1206.
86. J. Bhagwan, A. Sahoo, K. L. Yadav and Y. Sharma, *Electrochim. Acta*, 2015, **174**, 992–1001.
87. M. Singh, B. P. Dubey, A. Sahoo, K. L. Yadav and Y. Sharma, *J. Energy Storage*, 2021, **44**, 103361.
88. W. Tian, P. Ren, X. Hou, R. Xue, Z. Chen, Z. Guo, Y. Jin and F. Ren, *Int. J. Biol. Macromolec.*, 2024, **261**, 129977.
89. H. Wei, H. Gu, J. Guo, D. Cui, X. Yan, J. Liu, D. Cao, X. Wang, S. Wei and Z. Guo, *Adv. Compos. Hybrid Mater.*, 2018, **1**, 127–134.
90. S. Pal, S. Majumder, S. Dutta, S. Banerjee, B. Satpati and S. De, *J. Phys. D: Appl. Phys.*, 2018, **51**, 375501.
91. J. Zhu, M. Chen, H. Qu, Z. Luo, S. Wu, H. A. Colorado, S. Wei and Z. Guo, *Energy Environ. Sci.*, 2013, **6**, 194–204.
92. Z. Zeng, Y. Liu, W. Zhang, H. Chevva and J. Wei, *J. Power Sources*, 2017, **358**, 22–28.
93. G. Wang, H. Xu, L. Lu and H. Zhao, *J. Energy Chem.*, 2014, **23**, 809–815.
94. M. C. Fite, J.-Y. Rao and T. Imae, *Bull. Chem. Soc. Jpn.*, 2020, **93**, 1139–1149.
95. Y. Zhao, H. Li, R. Tang, X. Wang, Y. Wu, S. Yan and Y. Zhang, *J. Mater. Chem. A*, 2023, **11**, 15844–15854.
96. J. Zhao, K. Xu, W. Yang, Z. Wang and F. Zhong, *Chem. Soc. Rev.*, 2015, **44**, 8904–8939.
97. S. Altınışık, *ACS Omega*, 2026, **11**, 1826–1853.
98. F. Yi, H. Ren, K. Dai, X. Wang, Y. Han, K. Wang, K. Li, B. Guan, J. Wang, M. Tang, J. Shan, H. Yang, M. Zheng, Z. You, D. Wei and Z. Liu, *Energy Environ. Sci.*, 2018, **11**, 2016–2024.
99. M. M. Momeni, M. Najafi, H. Farrokhpour and B.-K. Lee, *J. Energy Storage*, 2024, **79**, 109666.

View Article Online
DOI: 10.1039/D6TA00650G

100. S. P. Madhusudanan, M. Suresh Kumar, K. Yamini Yasoda, D. Santhanagopalan and S. K. Batabyal, *J. Mater. Sci.: Mater. Electron.*, 2020, **31**, 752–761.
101. M. Zhu, Y. Huang, Y. Huang, Z. Pei, Q. Xue, H. Li, H. Geng and C. Zhi, *Adv. Funct. Mater.*, 2016, **26**, 4481–4490.
102. C. An, Z. Wang, W. Xi, K. Wang, X. Liu and Y. Ding, *J. Mater. Chem. A*, 2019, **7**, 15691–15697.
103. T. Fang, H. Hu, J. Liu, M. Jiang, S. Zhou, J. Fu, W. Wang and Y. Yang, *J. Phys. Chem. C*, 2021, **125**, 18734–18742.
104. B. Ezhilmaran, S. Madhavanunni Rekha and S. Venkataprasad Bhat, *Batteries & Supercaps*, 2025, **8**, e202400654.
105. W. Yang, J. Wang, S. Gao, H. Zhang, H. Wang and Q. Li, *J. Adv. Ceram.*, 2022, **11**, 1735–1750.
106. C. Yuan, H. Yin, H. Lv, Y. Zhang, J. Li, D. Xiao, X. Yang, Y. Zhang and P. Zhang, *JACS Au*, 2023, **3**, 3127–3140.
107. Y. Wang, H. Fang, S. Liang, X. Sheng, Y. Huang, Y. Zhang and Y. Zhou, *Appl. Surf. Sci.*, 2022, **606**, 154872.
108. B. D. Boruah and A. Misra, *ACS Appl. Energy Mater.*, 2019, **2**, 278–286.
109. T. Rao, Y. Zhou, J. Jiang, P. Yang and W. Liao, *Nano Energy*, 2022, **100**, 107479.
110. S. Kandpal, T. Ghosh, C. Rani, A. Chaudhary, J. Park, P. S. Lee and R. Kumar, *ACS Energy Lett.*, 2023, **8**, 1870–1886.
111. Y. Huang, B. Wang, F. Chen, Y. Han, W. Zhang, X. Wu, R. Li, Q. Jiang, X. Jia and R. Zhang, *Adv. Opt. Mater.*, 2022, **10**, 2101783.
112. D. Wei, M. R. J. Scherer, C. Bower, P. Andrew, T. Ryhänen and U. Steiner, *Nano Letters*, 2012, **12**, 1857–1862.
113. S. Wang, H. Xu, T. Hao, P. Wang, X. Zhang, H. Zhang, J. Xue, J. Zhao and Y. Li, *NPG Asia Mater.*, 2021, **13**, 51.
114. N. Ahlawat, L. Bansal, B. Sahu, D. K. Rath, S. Tiwari, A. Chaudhary, S. Kaladi Chondath and R. Kumar, *ACS Appl. Energy Mater.*, 2025, **8**, 4288–4298.
115. H. S. Chavan, B. Hou, A. T. A. Ahmed, Y. Jo, S. Cho, J. Kim, S. M. Pawar, S. Cha, A. I. Inamdar, H. Im and H. Kim, *Sol. Energy Mater. Sol. Cells*, 2018, **185**, 166–173.
116. Y. Wang, S. Wang, X. Wang, W. Zhang, W. Zheng, Y.-M. Zhang and S. X.-A. Zhang, *Nat. Mater.*, 2019, **18**, 1335–1342.
117. P. Shi, C. M. Amb, E. P. Knott, E. J. Thompson, D. Y. Liu, J. Mei, A. L. Dyer and J. R. Reynolds, *Adv.d Mater.*, 2010, **22**, 4949–4953.
118. S. Xiong, Y. Wang, X. Wang, J. Chu, R. Zhang, M. Gong, B. Wu and Z. Li, *Sol. Energy Mater. Sol. Cells.*, 2020, **209**, 110438.
119. K. Zhou, H. Wang, J. Jiu, J. Liu, H. Yan and K. Suganuma, *Chem. Eng. J.*, 2018, **345**, 290–299.
120. X. Chen, H. Lin, J. Deng, Y. Zhang, X. Sun, P. Chen, X. Fang, Z. Zhang, G. Guan and H. Peng, *Adv. Mater.*, 2014, **26**, 8126-8132.
121. Y. Xie, Y. Zhang, M. Zhu, R. Huang and D. Chao, *Dyes Pigm.*, 2023, **208**, 110889.
122. Y. Tian, S. Cong, W. Su, H. Chen, Q. Li, F. Geng and Z. Zhao, *Nano Letters*, 2014, **14**, 2150–2156.
123. P. Dutta, S. C. Karumuthil, R. Roy and A. K. Singh, *ACS Appl. Polym. Mater.*, 2023, **5**, 4088–4099.
124. G. Cai, P. Darmawan, M. Cui, J. Wang, J. Chen, S. Magdassi and P. S. Lee, *Adv. Energy Mater.*, 2016, **6**, 1501882.

125. X. Song, X. Dong, H. Liu, Z. Wang, Q. Cao, *ChemSusChem*, 2026, **19**, e202501440.

126. C. -Y. Hsu, F. Alnaimat, G. PadmaPriya, S. Al-Hasnaawei, M. Najafloo, M. Dehghanipour, S. Ray, K. Chennakesavulu, R. Sharma, A. S. Chauhan, *Mater. Today Chem.*, 2026, **51**, 103338.

127. Y. Kim, H. Bark, A. Gupta, Y. Zhang, J. lee, P. S. Lee, *Adv. Energy Mater.*, 2025, **15**, 2405480.

128. J. Kim, M. S. Kim, H. J. Kim, *Adv. Energy Mater.*, 2018, **8**, 1702028.

129. X. Wang, B. Liu, Q. Wang, *Chem. Soc. Rev.*, 2019, **48**, 162–191.

130. C. Yang, Z. Suo, *Nat. Rev. Mater.*, 2018, **3**, 125–142.

131. L. Hu, H. Wu, Y. Cui, *Energy Environ. Sci.*, 2011, **4**, 642–646.

132. D. -H. Kim, N. Lu, R. Ma, John A. Rogers, *Science*, 2011, **333**, 838–843.

View Article Online
DOI: 10.1039/D6TA00650G

Data availability statement

Data availability does not apply to this review paper as no new data are generated or analysed as part of this review.